

Exploring the Anticancer Potential of Diiron Bis-cyclopentadienyl Complexes with Bridging Hydrocarbyl Ligands: Behavior in Aqueous Media and *In Vitro* Cytotoxicity

Gabriele Agonigi,[#] Lorenzo Biancalana,[#] Maria Giovanna Lupo,[#] Monica Montopoli, Nicola Ferri,^{*} Stefano Zacchini, Francesca Binacchi, Tarita Biver, Beatrice Campanella, Guido Pampaloni, Valerio Zanotti,^{*} and Fabio Marchetti^{*}



Cite This: *Organometallics* 2020, 39, 645–657



Read Online

ACCESS |



Metrics & More

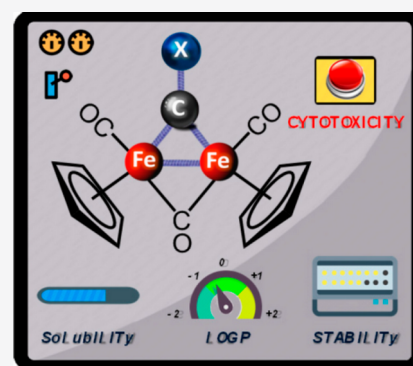


Article Recommendations



Supporting Information

ABSTRACT: A series of diiron complexes based on the $[\text{Fe}_2\text{Cp}_2(\text{CO})_x]$ skeleton ($\text{Cp} = \eta^5\text{-C}_5\text{H}_5$, $x = 2, 3$; $\eta^4\text{-C}_5\text{H}_5\text{Ph}$ in place of one Cp in one case) and containing different bridging hydrocarbyl ligands (aminocarbyne, thiocarbyne, allenyl) were preliminarily investigated for their anticancer potential. The water solubility, stability in water and in the presence of a cell culture medium, and octanol/water partition coefficient were evaluated by spectroscopic techniques. The cytotoxicity was assessed *in vitro* toward the human ovarian carcinoma cell line A2780, the human triple negative breast cancer cell line MDA-MB-231, and the human vascular smooth muscle cell line SMC. Some aminocarbyne complexes exhibited a potent cytotoxicity, with IC_{50} values in the low micromolar/nanomolar range, and a strong selectivity for the A2780 cells in comparison to the SMC cell line. Several experiments were carried out in order to give insight into the mode of action of selected compounds, including an assessment of catalytic NADH oxidation and ROS production and studies of binding with DNA and with a model protein.



INTRODUCTION

Across the quite large dimensional scale in which organometallic compounds can be classified, ranging from the atomic level to nanometer and micrometer length scales, dimetal complexes occupy a position very close to, although distinct from, monometal complexes. Indeed, dealing with dimetal complexes is not just a matter of “doubling” the average size of an organometallic compound. Complexes with a metal–metal interaction show a distinct character and chemical behavior, essentially due to two major reasons: (a) cooperative/synergic effects associated with the presence of two adjacent metal atoms and (b) the possibility of taking advantage of unique reactivity patterns provided by bridging coordination.¹ Our interest in this field has been focused on diiron complexes,² which indeed represent an area of growing attention for obvious reasons, mostly related to the urgent need to replace precious and toxic metals with more abundant and sustainable metals.³

The example which perhaps better illustrates how two adjacent metal centers may work in concert is given by the active site of the natural metallo-enzyme $[\text{FeFe}]$ -hydrogenase (Figure 1, structure I). In that case, the two Fe atoms cooperate, cutting in half the electronic requirements associated with the proton reduction to form H_2 , as well as the reverse reaction. The structure of the inorganic core of the

$[\text{FeFe}]$ -hydrogenase enzyme has inspired extensive investigations⁴ with the prospect that dihydrogen can become a major energy vector in the transition from fossil fuels to renewables. The prevalent focus has been so far on diiron complexes closely resembling the $[\text{FeFe}]$ -hydrogenase active site (i.e., dithiolate mimics, see structure II in Figure 1),⁵ although some of us have demonstrated that it is possible to extend these concepts to diiron complexes containing cyclopentadienyls and bridging hydrocarbyl ligands, which cannot be strictly considered as structural mimics but are able to provide new catalytic routes to H_2 evolution (functional mimics).⁶

Concerning the second distinctive feature of the dimetal complexes mentioned above (i.e., the bridging coordination), it has to be highlighted that organic fragments, when they bridge two transition-metal centers, may display reactivity patterns not accessible when the same fragments are bound to a single metal or are unbound. Examples are numerous, and regarding diiron species, the commercially available $\text{Fe}_2\text{Cp}_2(\text{CO})_4$ (1; $\text{Cp} = \eta^5\text{-C}_5\text{H}_5$) is a convenient starting material to obtain a large

Received: October 12, 2019

Published: February 14, 2020

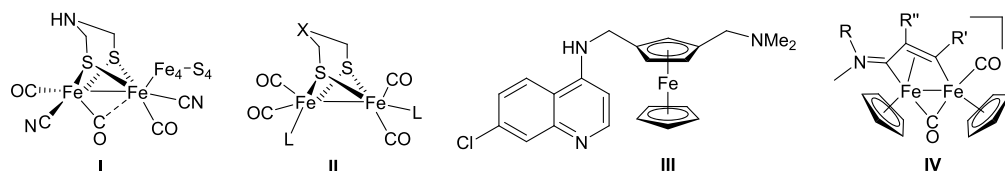
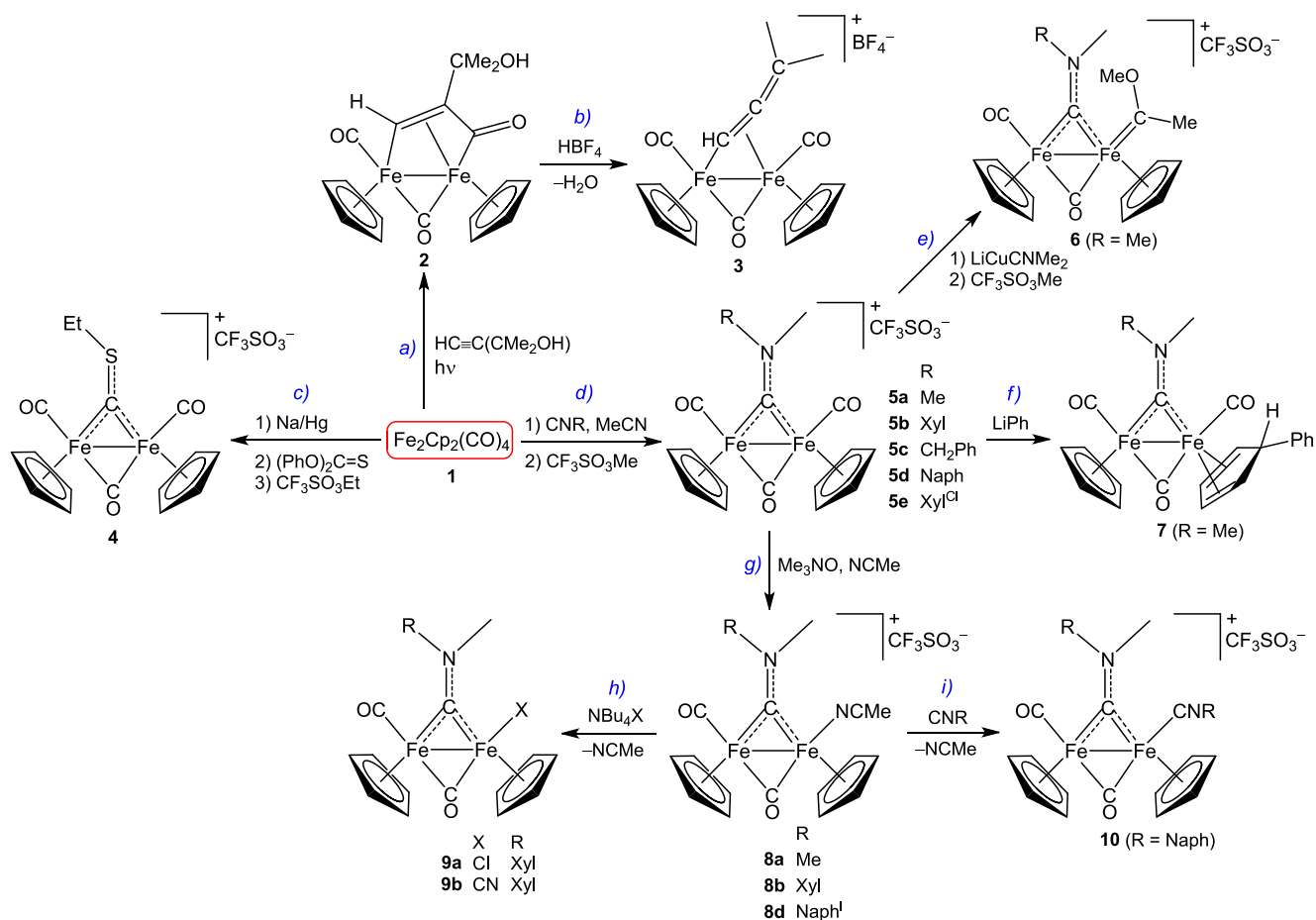


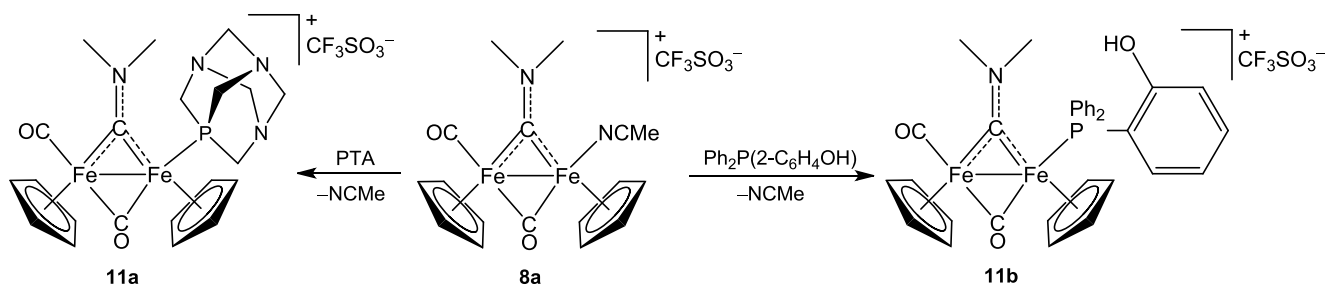
Figure 1. (I) Active site of hydrogenase. (II) Diiron complexes as synthetic models of hydrogenase (L = CN, phosphine, isocyanide, X = S, NH). (III) Ferroquine. (IV) Diiron vinyliminium complexes (triflate salts; R = alkyl, aryl, R' = H, alkyl, aryl, CO₂Me, R'' = H, alkyl).

Scheme 1. Synthetic Routes from Fe₂Cp₂(CO)₄ to Diiron Complexes with a Bridging Hydrocarbyl Ligand: (a) Vinyl Ketone by Photolytic Alkyne Insertion into an Fe–CO Bond;¹³ (b) Allenyl;¹⁴ (c) Thiocarbyne *via* Preliminary Generation of [FeCp(CO)₂][−];¹⁵ (d) Aminocarbyne (Xyl = 2,6-C₆H₃Me₂; Xyl^{Cl} = 2,6-C₆H₃Cl(Me); Naph = 2-naphthyl);¹⁶ (e) Aminocarbyne with a Terminal Alkoxyalkylidene Ligand;^{17,18} (f) Aminocarbyne with a Cyclopentadiene Ligand;^{20,19} (g) Aminocarbyne with a Labile Acetonitrile Ligand;²⁰ (h) Neutral Aminocarbyne with a (Pseudo)halide Ligand;¹⁸ (i) Aminocarbyne with a Terminal Isocyanide Ligand^{16a,21}



variety of unusual structural motifs: through the sequential elimination of CO ligands, it is possible to assemble and rearrange bridging coordinated organic fragments and to introduce functional groups up to building complex molecular architectures.^{2b,c,7} This amount of accumulated empirical data and numbers of synthetic routes constitute a huge potential for applications. In this regard, a promising area is the exploration of the possible use of iron complexes in medicinal chemistry. To date, ferrocene derivatives have emerged as the most promising candidates,⁸ and ferroquine, the ferrocene analogue of the antimalarial drug chloroquine (Figure 1, structure III), successfully completed two phase II clinical studies as an antimalarial agent⁹ and also revealed potent activity against

prostate cancer *in vivo*.¹⁰ Furthermore, Jaouen and co-workers have developed a series of ferrocenes derivatized with the drug hydroxytamoxifen (ferrocifens), displaying a significant cytotoxicity against a panel of cancer cell lines.¹¹ There are good reasons to believe that diiron bis-cyclopentadienyl complexes, which might be viewed as diiron analogues of ferrocene, could have a similar effect. In addition, they take full advantage of the very extended possibilities to design and modify the nature of the bridging hydrocarbyl ligand, providing the most appropriate substituents and functional groups in order to gain full control of fundamental properties for a metal-based drug (e.g., solubility, redox potential, stability, inertness or lability to ligand substitution). In this light, some of us recently reported

Scheme 2. Synthesis of μ -Aminocarbyne Complexes with a Terminal Phosphine Ligand^a

^aPTA = 1,3,5-triaza-7-phosphatricyclo[3.3.1.1]decane.

about the antiproliferative activity of diiron vinyliminium complexes (Figure 1, structure IV), representing the first family of organo-diiron complexes proposed as possible anticancer agents.¹²

In order to extend the library of diiron complexes potentially able to act as metal drugs, we decided to consider a variety of compounds available from **1** (Scheme 1). Herein, we will present a screening study aimed to assess the adaptability of these compounds to an aqueous environment and to preliminarily evaluate their *in vitro* cytotoxicity.

RESULTS AND DISCUSSION

Synthesis and Characterization of Compounds.

Compounds **3–10** were synthesized following the respective literature procedures under anhydrous conditions and a N_2 atmosphere (Scheme 1), with the exception of **8a**, which was obtained by adopting a novel, simplified method (see the Experimental Section for details). The unprecedented aminocarbyne complexes **11a,b** were synthesized from **8a** via acetonitrile/phosphine substitution and isolated in 85–90% yields after chromatographic purification (Scheme 2).

Complex **11a** contains the amphiphilic PTA ligand, which has been incorporated in a variety of ruthenium and platinum complexes designed as anticancer agents, in order to enhance their water solubility and provide stability to the organometallic structures.^{22,23} In particular, the family of Ru(II) arene compounds $[\text{RuCl}_2(\eta^6\text{-arene})(\kappa\text{P-pta})]$ (RAPTA complexes) have emerged as promising drug candidates.²⁴ Complex **11a** was obtained as a mixture of two isomers (ratio 5:1), which were attributed to the *cis* and *trans* mutual geometries of the Cp rings. A fraction of the prevalent *cis*-**11a** was isolated from a CHCl_3 solution of the mixture. The occurrence of a *cis* to *trans* rearrangement on going from the aminocarbyne adducts **8a,b** to a variety of acetonitrile-substitution products was previously described.²⁵

The IR spectra of **11a,b** (in CH_2Cl_2 solution) exhibit a typical pattern consisting of two intense bands due to the terminal and bridging carbonyl ligands, respectively (e.g., at 1992 and 1788 cm^{-1} in the case of **11b**), and one additional absorption related to the carbyne–nitrogen bond, at around 1580 cm^{-1} . As a consequence of the partial double-bond character of this linkage, the N substituents are nonequivalent and resonate at 55.3 and 51.7 ppm in the ^{13}C NMR spectrum of **11b** (acetone- d_6 solution). The aminocarbyne carbon manifests itself by a characteristic downfield ^{13}C NMR resonance (326.6 ppm in **11b**),^{2b,16,25a,26} split into a doublet ($^2J_{\text{CP}}$ ca. 15 Hz) due to coupling with the phosphorus atom. The same effect is observed for the bridging ($^2J_{\text{CP}}$ ca. 15 Hz) but not the terminal ($^3J_{\text{CP}}$ ca. 0–2 Hz) carbonyl ligand. The

different orientations of the Cp ligands in the two isomers of **11a** were unambiguously ascertained by an ^1H NOE experiment. Thus, irradiation of one Cp resonance related to *cis*-**11a** (δ_{H} 5.27 ppm) evidenced a NOE interaction with the other Cp (δ_{H} 5.14 ppm), whereas irradiation of either Cp (δ_{H} 5.21 and 5.05 ppm) belonging to *trans*-**11a** revealed the mutual absence of an NOE effect. In the ^{31}P NMR spectrum of **11a**, the phosphorus nucleus resonates at -21.8 ppm (*cis*-**11a**) and -13.1 ppm (*trans*-**11a**) respectively, these values falling within the range typical for a P-coordinated PTA ligand.^{23,27,28}

In order to obtain crystals suitable for X-ray analysis, diethyl ether was allowed to slowly diffuse into a solution of **11a** in methanol, to which a few grains of NaCl were added to favor crystallization. The structure of $[\text{Fe}_2\text{Cp}_2(\text{CO})(\mu\text{-CO})\{\mu\text{-CNMe}_2\}(\text{PTA})]\text{Cl}$ (**11a**^{Cl}) was therefore ascertained by a X-ray diffraction study (Figure 2 and Tables S1 and S2). The

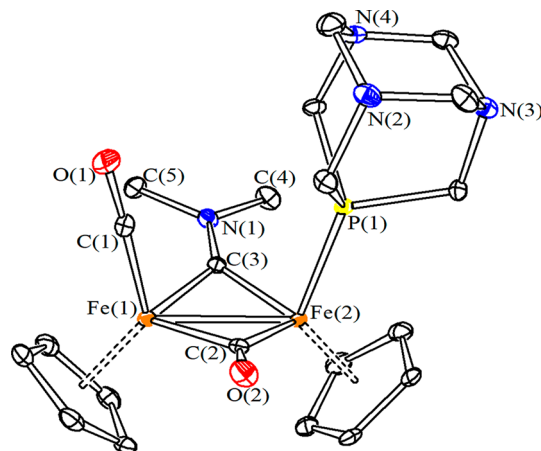


Figure 2. View of the structure of the cation within **11a**^{Cl}. Displacement ellipsoids are at the 50% probability level. Hydrogen atoms have been omitted for clarity.

geometry and bonding parameters within the $[\text{Fe}_2\text{Cp}_2(\mu\text{-CNMe}_2)(\text{CO})(\mu\text{-CO})]$ core are quite comparable to those previously reported for analogous diiron μ -aminocarbyne complexes.^{2b,16,21,29} More precisely, the Fe(1)–Fe(2) length (2.5195(4) Å) is consistent with the presence of a single bond, while the C(3)–N(1) distance (1.306(3) Å) reveals a considerable double-bond character, in agreement with the spectroscopic data (see above). Therefore, the μ -aminocarbyne can be alternatively described as a bridging iminium ligand, and N(1) displays an almost perfect sp^2 hybridization (sum of the angles at N(1) 359.9(3)°). The NMe_2 unit is slightly tilted with respect to $\text{Fe}_2(\mu\text{-C})$ (dihedral angles Fe(1)–C(3)–

N(1)–C(5) 5.22° and Fe(2)–C(3)–N(1)–C(4) 5.33°, and the Cp ligands adopt a *cis* geometry, as is often found in similar complexes.^{2b,16,29,30} The Fe(2)–P(1) distance (2.2088(6) Å) compares well with that found in analogous diiron complexes containing a terminal PTA ligand.^{27a,b,31}

Behavior in Aqueous Media: Solubility, Stability, and Octanol/Water Partition Coefficient. The water solubility of the diiron compounds 3–11 was assessed in saturated D₂O solutions at 21 °C by ¹H NMR spectroscopy, using dimethyl sulfone as an internal standard: data are compiled in Table 1.

Table 1. Solubility in Water (D₂O) and Octanol/Water Partition Coefficient (log *P*_{ow}) for Diiron Complexes^a

compd	D ₂ O solubility/mol L ⁻¹	log <i>P</i> _{ow}
3	ca. 3 × 10 ⁻³ ^c	n.d. ^c
4	5.8 × 10 ⁻³	-0.9 ± 0.1
5a ^b	3.2 × 10 ⁻³	-0.9 ± 0.1
5b	1.4 × 10 ⁻³	-0.27 ± 0.04
5c	2.9 × 10 ⁻³	-0.51 ± 0.02
5d	not soluble ^d	0.29 ± 0.03
5e ^b	not soluble ^d	-0.09 ± 0.07
6	ca. 8 × 10 ⁻⁴	-0.9 ± 0.1
7	not soluble ^d	>2
9a ^b	not soluble ^d	>2
9b ^b	not soluble ^d	>2
10 ^b	not soluble ^d	1.2 ± 0.1
<i>cis</i> -11a	4.6 × 10 ⁻²	<-2
11b	ca. 5 × 10 ⁻⁴	1.0 ± 0.1

^aAll data refer to *T* = 21 °C. ^bData are referred to all isomers collectively. ^cRapid degradation in water (*vide infra*). ^dSolubility below the lowest value of quantitation (ca. 3 × 10⁻⁴ M).

All of the ionic compounds display an appreciable water solubility (≥10⁻³ mol L⁻¹), except for those bearing 2-naphthyl (5d, 10) or 2,6-C₆H₃Cl(Me) (5e) groups. The PTA complex *cis*-11a possesses the highest solubility: 4.6 × 10⁻² M, corresponding to ca. 30 g L⁻¹; as a comparison, the solubility of cisplatin in H₂O is estimated to be 3 g·L⁻¹.³²

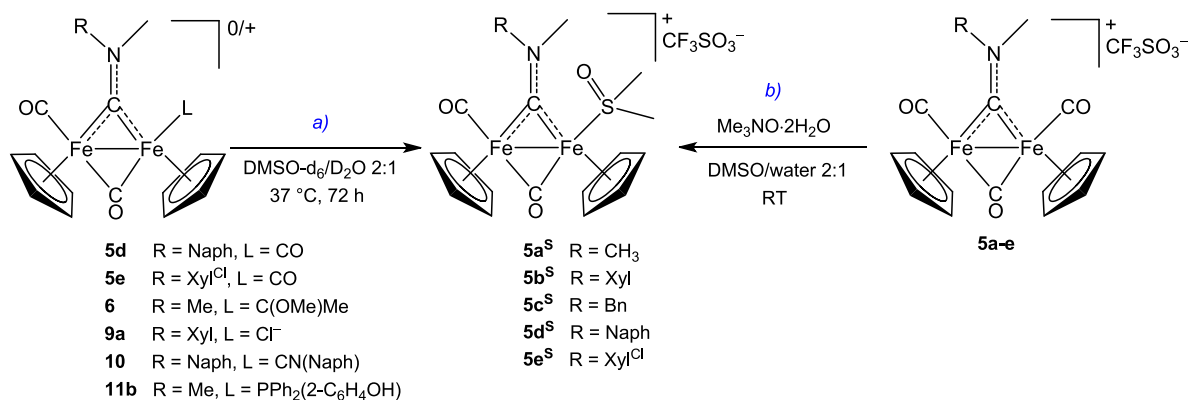
Octanol/water partition coefficients (log *P*_{ow}; Table 1) of 3–11 were spectrophotometrically assessed using the shake-flask method (see the Experimental Section for details). The majority of the compounds show an amphiphilic character, with log *P*_{ow} ranging from -0.9 to 1.0. Hydrophilicity is favored by the presence of small alkyl substituents on the

nitrogen atom (aminocarbyne ligand) or on the sulfur atom (thiocarbyne ligand), as in 4, 5a, and 6 (log *P*_{ow} = -0.9). The effect of the presence of the PTA ligand in *cis*-11a results in log *P*_{ow} < -2. In contrast, the neutral compounds 7 and 9a,b show considerable hydrophobicity (log *P*_{ow} > 2).

The stability of the water-soluble compounds 3, 4, 5a–d, and *cis*-11a in D₂O solution at 37 °C was monitored over time by ¹H NMR spectroscopy (Table S3). The allenyl derivative 3 underwent quick changes upon dissolution, leading to quantitative precipitation of a brown solid within a few hours. The notable instability of 3 seems ascribable to the μ-η¹:η² coordination mode of the allenyl ligand, presumably allowing the entrance of water into the metal coordination sphere by displacement of the coordinated C=C π system. Analogously, a μ-η¹:η²-vinyl analogue of 3 was reported to readily break into monoiron species by addition of acetonitrile.³³ On the other hand, a single set of ¹H/³¹P NMR signals was observed for freshly prepared solutions of 4, 5a–d, and *cis*-11a, assigned to the starting materials.³⁴ In these cases, a small amount of an orange-brown precipitate was observed after 72 h; the precipitates recovered from 5a,b were identified as hematite (Fe₂O₃) and a mixture of hematite (Fe₂O₃) and magnetite (Fe₃O₄), respectively (Raman analyses). A considerable fraction of the starting material (51–75%) was found in the NMR spectra of the final solutions, and no additional {FeCp} species was identified. In the case of 11b, release of a phosphine oxide (O=PTA) was detected. Stability experiments were also performed on 4 and 5a–e in a D₂O/CD₃OD mixture, the compounds generally showing a stability higher (65–83%) than that in D₂O (experimental details in the Supporting Information).

For those compounds featured by low water solubility, i.e. 5d,e, 6, 7, 9a,b, 10 and 11b, stability experiments were conducted in DMSO-*d*₆/D₂O 2/1 v/v solution. Thus, a variable amount (0–78%) of starting material was detected by ¹H NMR after storing the solutions at 37 °C for 72 h (Table S4). Newly formed {FeCp} species were also recognized, the prevalent one being identified as the DMSO adduct [Fe₂Cp₂(CO)(μ-CO){μ-CNMeR}(DMSO)]⁺ (5a–e^S; Scheme 3a). The formation of 5a–e^S appears to be the result of substitution of respectively monodentate carbonyl (5d,e), carbene (6), chloride (9a), isocyanide (10), and phosphine (11b) ligands with DMSO. Accordingly, 5a–e^S were also obtained by treating DMSO-*d*₆/D₂O 2/1 v/v solutions of 5a–

Scheme 3. Formation of Aminocarbyne-DMSO Complexes 5a–e^S from (a) DMSO/Water Solutions of 5d,e, 6, 9a, 10, and 11b at 37 °C and (b) Reaction of 5a–e with Me₃NO·2H₂O in DMSO/Water



e with $\text{Me}_3\text{NO}\cdot 2\text{H}_2\text{O}$, as a decarbonylating agent (Scheme 3b). Following the latter procedure, **5b^S** was isolated in 77% yield by CH_2Cl_2 /water extraction and characterized by IR and NMR spectroscopy. The DMSO ligand in **5b^S** gives rise to a strong IR band at 1107 cm^{-1} , related to the sulfoxide group, and NMR resonances due to the inequivalent *S*-methyls at 3.4–3.5 (^1H) and 50–55 ppm (^{13}C).

Next, the stability of diiron compounds was investigated in the presence of a cell culture medium (see the Experimental Section for details). Solutions of **4–6** and **9–11** (ca. 10^{-3} M) in DMSO/cell culture medium mixtures were maintained at 37°C for 72 h and then diluted with water and extracted with CH_2Cl_2 . The observed turbidity in the aqueous phase suggests some degradation to iron oxides, consistent with what was found in D_2O . The residue of the organic phase was analyzed by IR and NMR spectroscopy, and the starting material was identified as the major species in most cases. Considerable degradation was observed only for **5e** and **6**, whereas **9a** showed higher stability than in DMSO/water, presumably due to the high chloride concentration typical of the cell medium, inhibiting Cl^- dissociation from the complex. A gas-chromatographic analysis of the reaction atmosphere, in the cases of **5b** and **9a**, clearly evidenced the production of carbon monoxide, in agreement with the extensive fragmentation of the diiron frame (see above).

Cytotoxic Activity and Iron Cellular Uptake. To determine the cytotoxic activity of the diiron complexes, we incubated the human triple negative breast cancer cell line (MDA-MB-231) and the human ovarian carcinoma cell line (A2780), respectively, with increasing concentrations of the compounds. The cell viability was assessed after 48 h by a sulforhodamine assay (SRB) (see Table 2). Cisplatin was used as a positive control. A series of compounds, i.e. **5d,e**, **7**, **9a**, **10**, and **11b**, are able to potentially inhibit cell proliferation on both cancer cell lines, being more effective than cisplatin especially against the MDA-MB-231 cells. In general, the cytotoxicity appears more oriented toward the A2780 cell line, except for **3**,

Table 2. IC_{50} Values (μM) Determined for Diiron Compounds and Cisplatin on Human Ovarian Carcinoma (A2780), Human Triple Negative Breast Cancer (MDA-MB-231), and Human Vascular Smooth Muscle Cell (hSMC) Cell Lines after 48 h Exposure^a

compd	A2780	MDA-MB-231	hSMCs
1	41 ± 4	>200	107 ± 3
3	79.1 ± 1.0	55 ± 8	125 ± 4
4	42.1 ± 1.8	128.7 ± 1.2	>200
5a	>200	>200	>200
5b	9.3 ± 0.7	55 ± 8	>200
5c	9.6 ± 1.5	51 ± 9	24.1 ± 0.8
5d	1.45 ± 0.04	13.0 ± 0.5	19.9 ± 1.1
5e	2.30 ± 0.03	14 ± 9	18.8 ± 1.0
6	69 ± 7	188 ± 6	>200
7	2.2 ± 0.4	8.9 ± 0.8	6.3 ± 1.8
9a	12 ± 3	7 ± 4	14.4 ± 1.5
9b	46 ± 5	>200	>200
10	0.11 ± 0.04	2.8 ± 1.5	6.31 ± 0.01
11a	>200	>200	>200
11b	9.2 ± 0.3	8.5 ± 1.1	12.6 ± 0.3
cisplatin	6 ± 4	99 ± 35	7 ± 4

^aValues are given as the mean ± SD.

9a, and **11b**. In order to evaluate a possible degree of selectivity with respect to primary cells, we tested the cytotoxicity of the complexes also on human vascular smooth muscle cells (hSMCs). Thus, **5b,d,e** and **10** showed a much stronger cytotoxic effect on A2780 cancer cells rather than hSMCs. The lack of selectivity displayed by **3** may be related to the fast degradation of this complex in water media (see above).

The accumulation of iron in MDA-MB-231 cells was quantified by inductively coupled plasma mass spectrometry (ICP-MS), after incubation of MDA-MB-231 cells with four selected compounds, i.e. **5a,b**, **7**, and **9b** (Table 3). Incubation

Table 3. Iron Uptake in MDA-MB-231 Cells after Incubation with Diiron Complexes at Variable Concentrations

compd	cellular uptake ($10^{-8}\text{ g Fe/mg protein}$)	
	50 μM	100 μM
5a	23 ± 4	34 ± 11
5b	64 ± 2	103 ± 9
7	14 ± 4 ^b	23 ± 8 ^c
9b	23 ± 6	34 ± 13
blank ^a	16 ± 3	

^aIron content determined in untreated cells. ^b5 μM . ^c10 μM .

with **5b** ($\log P = -0.27$, Table 1) led to a significant, dose-dependent accumulation of iron into the cells. Conversely, a modest iron uptake was observed for **5a** ($\log P = -0.9$) and **9b** ($\log P > 2$) at the highest level of incubation (100 μM). These results suggest that an amphiphilic character may be beneficial to the cellular uptake of diiron compounds and the associated cytotoxic effects (Table 2). Incubation with the lipophilic but poorly stable compound **7** at concentrations near the IC_{50} value did not produce a significant iron uptake.

Relevant to the cytotoxic activity, we evaluated the effect of **5b** (highly cytotoxic) and **9b** (moderately cytotoxic) on the p53 mRNA levels in A2780 cells, using cisplatin as a positive control. Indeed, the p53 protein is considered a linker to DNA repair and a checkpoint activator of the cell cycle and apoptosis processes observed in response to cisplatin.³⁵ Therefore, cytotoxic compounds able to activate these pathways are expected to induce p53 expression; in fact, our experiments showed that both **5b** and **9b** induce p53 mRNA expression on the A2780 cell line (Figure 3).

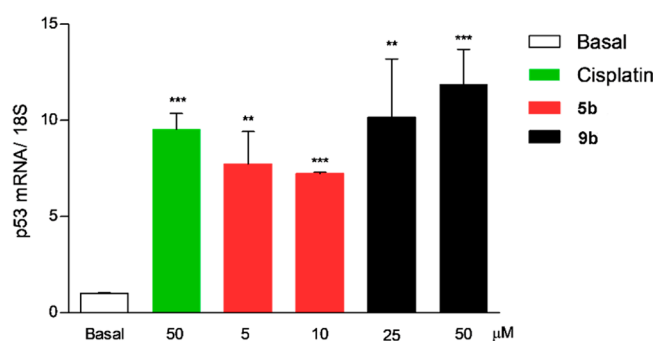


Figure 3. Effect of select diiron complexes and cisplatin (at different concentrations) on p53 mRNA levels (A2780 cell line). Results are represented as gene of interest/housekeeping ratio and compared to the basal condition (* $p < 0.05$; ** $p < 0.01$; *** $p < 0.001$ vs. basal).

Redox Chemistry. Former voltammetric studies conducted on acetonitrile solutions of the cationic carbyne complexes **4** and **5a,b** evidenced reversible reduction processes occurring respectively at -1.20 , -1.40 , and -1.40 V (vs the ferrocenium/ferrocene couple).³⁶ Experiments carried out under analogous conditions on some diiron vinyliminium complexes (Figure 1, IV) provided comparable reduction potential values,^{36,37} and it has been hypothesized that the mono-electron reduction of the latter species in the cells is implicated in their antiproliferative activity.^{12,38} Furthermore, it is well documented that the one-electron reduction of **4** enhances the reactivity of this complex, and in particular the CO ligands become more labile and thus susceptible to fast substitution reactions.³⁹ In combination, these features suggest that the reduction of cationic thiocarbyne (**4**) and aminocarbyne complexes (**5**, **6**, **10**, **11**) might play a role in their cytotoxic activity. On the other hand, the reduction potential of neutral aminocarbyne complexes (**7**, **9**), due to the absence of a net positive charge, is expected to be rather prohibitive,^{36,40} whereas the oxidation might become a feasible process in physiological medium.⁴¹

In addition to the possible reduction/oxidation of cationic/neutral complexes, also the slow decomposition in aqueous solutions, releasing the Fe(II) centers and then converting into Fe(III) oxide (see above), is expected to affect the redox balance in the cells, contributing to the cytotoxicity of the complexes. In fact, the decay of ferrocene-based prodrug candidates into Fe(II) ions was previously found to play an important role in their cytotoxic activity.⁴²

Therefore, we performed some experiments aimed to highlight the influence of selected diiron complexes on cell redox mechanisms. Nicotinamide adenine dinucleotide (NAD⁺) and its reduced form (NADH) are important cofactors contributing to the maintenance of the redox balance in cells,⁴³ and the alteration of the NADH/NAD⁺ ratio has been recently implicated in the anticancer activity of Os(II) and Ir(III) half-sandwich complexes.⁴⁴ Therefore, aerobic oxidation of NADH in the presence of select diiron compounds (**5a,b,d** and **9a,b**) was evaluated by UV-vis monitoring in water/methanol solutions kept at 37 °C, according to a previously documented procedure (Table 4).^{44b} Iron(II) sulfate was used as a reference. The cationic aminocarbyne compounds **5a,b,d** showed a moderate catalytic effect on NADH oxidation, while the neutral compounds **9a,b** were substantially ineffective.

In addition, we investigated the potential of selected complexes to influence the production of intracellular reactive oxygen species (ROS), by means of fluorescence measure-

ments using the DCFH-DA assay.⁴⁵ Thus, MDA-MB-231 cells were incubated with H₂-DCF-DA and with **5a,b**, **7**, and **9b**, respectively: in general, under the employed conditions,¹² there is no evidence that the compounds are able to significantly induce the production of ROS (Figure 4).

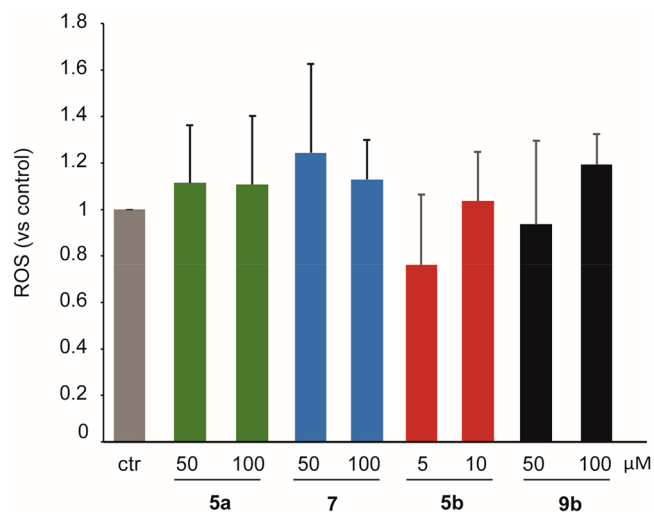


Figure 4. Effect of selected diiron complexes on ROS production in MDA-MB-231 cell line. Cells were incubated for 24 h with indicated concentrations of complexes. Results are represented as fold changes in comparison to control untreated cells (ctr).

Interaction of 5b with Biomolecules. The interaction of the cytotoxic aminocarbyne complex **5b** with potential biomolecular targets was investigated to give insights into the mechanism of action. The interaction with DNA was tested by ethidium bromide (EB) displacement: first, calf thymus DNA was saturated with EB, producing the known fluorescence emission increase at the wavelengths typical of the EB/DNA intercalated species ($\lambda_{\text{ex}} = 520$ nm, $\lambda_{\text{em}} = 595$ nm). Then, **5b** was added to the mixture and fluorescence emission changes were monitored. The observed moderate fluorescence decrease indicates the occurrence of weak **5b**/DNA interactions (Figure S1).

In addition, the affinity of **5b** to bovine serum albumin (BSA) was studied by performing spectrofluorimetric titrations, where aliquots of the complex were added to a BSA solution ($\lambda_{\text{ex}} = 280$ nm, $\lambda_{\text{em}} = 345$ nm). The observed decrease in BSA fluorescence emission (Figure S2A) occurred with a high Stern–Volmer constant, $K_{\text{SV}} = (9.1 \pm 0.3) \times 10^4$, whose magnitude order agrees with the static quenching of the protein emission and thus suggests adduct formation between **5b** and BSA.⁴⁶ Data were plotted using an alternative form of the Scatchard equation,⁴⁷ indicating a 1/1 stoichiometry for such an adduct (for details, see Figures S2B and S3 and eq S1 in the Supporting Information).

CONCLUSIONS

Monoiron compounds have aroused considerable interest due to their possible pharmacological use, and some ferrocene derivatives have clearly emerged in this field. On the other hand, analogous studies on diiron compounds remain almost absent in the literature. Traditional organometallic chemistry has provided access to a wide variability of structural motifs and related properties, starting from the easily available $\text{Fe}_2\text{Cp}_2(\text{CO})_4$, exploiting reactivity patterns hardly available

Table 4. Turnover Numbers (TONs) of **5a,b,d**, **9a,b**, and FeSO_4 (10 μM) in the Aerobic Oxidation of NADH (220 μM) in a 95/5 v/v H₂O/MeOH Solution at 37 °C after 26 h

compd	TON (26 h)
5a	4.9
5b	4.4
5d	5.5
9a	2.8 ^a
9b	2.6 ^a
FeSO_4	2.6 ^a

^aNADH conversion is not significantly different from the blank experiment.

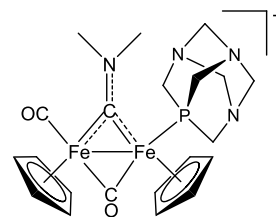
on analogous mononuclear species. This arsenal of compounds, which might be viewed as dinuclear analogues of ferrocenes, holds an intriguing but unexplored potential in terms of medicinal applications. In this light, the behavior of a selection of complexes based on the $[\text{Fe}_2\text{Cp}_2(\text{CO})_x]$ core and containing a bridging hydrocarbonyl ligand was evaluated for the first time. The compounds displayed a variable stability in water and in the presence of a cell culture medium and were investigated for their antiproliferative activity toward a panel of cell lines. Complexes containing a bridging aminocarbyne ligand, featuring fair water stability and a good balance between hydrophilicity and lipophilicity, exhibit the best cytotoxicity patterns, including a significant selectivity against cancer cells in comparison to normal cells. The action of these compounds seems multimodal, including interaction with proteins and, possibly, interference with redox processes (moderate catalytic effect on NADH oxidation), but not significant DNA binding. Also the observed, slow degradation of the complexes in water, leading to extensive disruption of the diiron frame, may be functional to the cytotoxicity; in particular, although deeper studies would be needed to clarify this latter point, carbon monoxide, dissociated from coordination, might exert some activity complementary to the anticancer effect.⁴⁸ The antiproliferative action of cationic diiron compounds described in this work and containing a C¹ bridging ligand appears somehow different from that of related diiron complexes with a bridging C³ vinyliminium ligand, the latter clearly triggering ROS production and being almost unreactive toward model proteins.¹²

EXPERIMENTAL SECTION

Materials and Methods. Syntheses were carried out under a nitrogen atmosphere using standard Schlenk techniques; all other operations were conducted in air with common laboratory glassware. When required, reaction vessels were oven-dried at 140 °C prior to use, evacuated (10^{-2} mmHg), and then filled with nitrogen. Organic reactants (TCI Europe or Merck) and $\text{Fe}_2\text{Cp}_2(\text{CO})_4$ (Strem; Cp = $\eta^5\text{-C}_5\text{H}_5$) were commercial products of the highest purity available. Compounds **3**,^{14a} **4**,^{15a} **5a–e**,^{16a} **6**,¹⁸ **7**,¹⁹ **9a,b**,²⁰ and **10**^{16a} were prepared according to published procedures. Solvents were distilled before use under nitrogen from appropriate drying agents. Chromatography separations were carried out on columns of deactivated alumina (Merck, 4% w/w water). Infrared spectra of solid samples were recorded on a PerkinElmer Spectrum One FT-IR spectrometer, equipped with a UATR sampling accessory. Infrared spectra of solutions were recorded on a PerkinElmer Spectrum 100 FT-IR spectrometer with a CaF₂ liquid transmission cell (2300–1500 cm^{-1} range). NMR spectra were recorded at 298 K on a Bruker Avance II DRX400 instrument equipped with a BBFO broad-band probe. Chemical shifts (expressed in parts per million) are referenced to the residual solvent peaks⁴⁹ (¹H, ¹³C) or to external standard (¹⁹F to CCl₃F, ³¹P to 85% H₃PO₄). NMR spectra were assigned with the assistance of ¹H–¹³C (gs-HSQC and gs-HMBC) correlation experiments.⁵⁰ Raman analysis was conducted with a Renishaw Invia micro-Raman instrument equipped with a Nd:YAG laser working at 532 nm and 0.1 mW, with an integration time of 10 s. Carbon, hydrogen, and nitrogen analyses were performed on a Vario MICRO cube instrument (Elementar). GC analyses were performed on a Clarus 500 instrument (PerkinElmer) equipped with a 5 Å MS packed column (Supelco) and a TCD detector. Samples were analyzed by isothermal runs (120 °C, 4 min) using He as a carrier gas. Synthesis and characterization of compounds (Charts 1–3).

cis-/trans-[Fe₂Cp₂(CO)(μ-CO){μ-η¹-CNMe₂}(κP-PTA)]-CF₃SO₃ (11a**).** Compound **8a** was preliminarily prepared by a slight modification of the literature procedure:²⁰ a solution of **5a** (174 mg, 0.277 mmol) in deaerated acetonitrile (15 mL) was allowed to react

Chart 1. Structure of the Cation of *cis*-**11a**

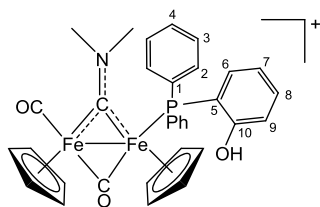


with Me₃NO·2H₂O (30 mg, 0.27 mmol). After 1 h, the IR spectrum recorded on an aliquot of the darkened solution indicated the clean formation of **8a**. The solvent was removed under vacuum. The dark brown residue was dissolved in acetone (8 mL), and then PTA (1,3,5-triaza-7-phosphatricyclo[3.3.1.1]decane; 43 mg, 0.27 mmol) was added. The dark brown solution was stirred at reflux temperature under N₂ for 2 h, progressively turning to dark green. The conversion was checked by ³¹P NMR, and then the volatiles were removed under vacuum. The residue was dissolved in a small volume of MeCN and charged on an alumina column (height 6 cm, diameter 2.3 cm). Impurities were eluted with MeCN, and then a green band was eluted using MeCN/MeOH 10/1 v/v. Volatiles were removed under vacuum (40 °C), affording **11a** as a dark green solid (*cis/trans* ratio 5/1; ¹H/³¹P NMR in acetone-*d*₆). Yield: 152 mg, 84%. Subsequently, the mixture of isomers was suspended in CHCl₃ (10 mL) and filtered. The dark green solid that was obtained was thoroughly washed with CHCl₃ and then Et₂O, affording pure *cis*-**11a** (¹H/³¹P NMR in acetone-*d*₆). The solid was dried under vacuum (40 °C) and stored under N₂ (slightly hygroscopic). Yield: 69 mg, 38%. Compound *cis*-**11a** is soluble in water, MeOH, and MeCN, less soluble in acetone, poorly soluble in CH₂Cl₂ and CHCl₃, and insoluble in toluene and Et₂O. Anal. Calcd for C₂₂H₂₈F₃Fe₂N₄O₅PS: C, 40.02; H, 4.27; N, 8.49. Found: C, 39.85; H, 4.37; N, 8.50. IR (solid state): $\tilde{\nu}/\text{cm}^{-1}$ 3566w, 3089w, 3067w-sh, 2933w, 2880w-sh 1976m-sh (CO), 1952s (CO), 1815w-sh, 1787s (μ -CO), 1781s (μ -CO), 1665w, 1572m (μ -CN), 1448w, 1422w, 1392w, 1261s, 1246s-sh, 1221m-sh, 1193w, 1160s, 1148s, 1105m, 1046w, 1028s, 1020s-sh, 973s, 950s, 897w, 877m, 853m, 842m-sh, 831w, 807m, 763s, 764s. IR (MeCN): $\tilde{\nu}/\text{cm}^{-1}$ 1966s (CO), 1799s (μ -CO), 1572m (μ -CN). ¹H NMR (acetone-*d*₆): δ/ppm 5.27 (s, 5H, Cp), 5.14 (d, ³J_{HP} = 1.5 Hz, 5H, Cp'), 4.38–4.33 (m, 6H, NMe + NCH₂), 4.31–4.26 (m, 6H, NMe' + NCH₂), 3.94–3.82 (m, 6H, PCH₂). ¹³C{¹H} NMR (acetone-*d*₆): δ/ppm 324.4 (d, ²J_{CP} = 17 Hz, μ -CN), 263.1 (d, ²J_{CP} = 17 Hz, μ -CO), 216.3 (CO), 89.9 (Cp), 87.9 (Cp'), 72.9 (d, ³J_{CP} = 7 Hz, NCH₂), 54.5 (PCH₂), 54.4, 54.2 (NMe₂). ¹⁹F{¹H} NMR (acetone-*d*₆): δ/ppm 78.8. ³¹P{¹H} NMR (acetone-*d*₆): δ/ppm -22.0. ¹H NMR (CD₃OD): δ/ppm 5.18 (s, 5H, Cp), 5.03 (d, ³J_{HP} = 1.2 Hz, 5H, Cp'), 4.40 (d, ²J_{HH} = 13.2 Hz, 3H, NCH₂), 4.30 (d, ²J_{HH} = 13.1 Hz, 3H, NCH₂), 4.22 (s, 3H, NMe₂), 4.18 (s, 3H, NMe₂), 3.84–3.75 (m, 6H, PCH₂). ³¹P{¹H} NMR (CD₃OD): δ/ppm -20.2.

trans-11a (in Admixture with cis-11a). IR (CH₂Cl₂): $\tilde{\nu}/\text{cm}^{-1}$ 1965vs (CO), 1799s (μ -CO), 1575m (CN). IR (THF): $\tilde{\nu}/\text{cm}^{-1}$ 1960vs (CO), 1779s (μ -CO), 1579m (μ -CN). ¹H NMR (acetone-*d*₆): δ/ppm 5.21 (s, 5H, Cp), 5.05 (d, ³J_{HP} = 1.4 Hz, 5H, Cp'), 4.47–4.39 (m, 9H, NCH₂/NMe). ³¹P{¹H} NMR (acetone-*d*₆): δ/ppm -18.1. ¹H NMR (D₂O): δ/ppm 5.12 (s, 5H, Cp), 4.96 (d, ³J_{HP} = 1.3 Hz, 5H, Cp). ³¹P{¹H} NMR (D₂O): δ/ppm -13.1.

A few X-ray-quality crystals of $[\text{Fe}_2\text{Cp}_2(\text{CO})(\mu\text{-CO})\{\mu\text{-CNMe}_2\}\{\mu\text{-CNMe}_2\}\{\mu\text{-CNMe}_2\}(\text{PTA})]\text{Cl}$ (**11a**^{Cl}) were collected by slow diffusion of diethyl ether into a methanol solution of **11a** and NaCl at room temperature.

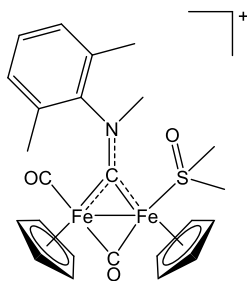
[Fe₂Cp₂(CO)(μ-CO){μ-η¹-CNMe₂}(κP-Ph₂P(2-C₆H₄OH))]-CF₃SO₃ (11b**).** The title product was prepared by using a procedure analogous to that described for **11a**, from **5a** (200 mg, 0.377 mmol) and Ph₂P(2-C₆H₄OH) (157 mg, 0.564 mmol). The acetone solution was refluxed for 5 h. Green solid, yield 85%. Anal. Calcd for C₃₄H₃₁F₃Fe₂NO₆PS: C, 52.26; H, 4.00; N, 1.79. Found: C, 52.12; H, 4.05; N, 1.88. IR (CH₂Cl₂): $\tilde{\nu}/\text{cm}^{-1}$ 1992vs (CO), 1788s (μ -CO), 1586m (μ -CN). IR (THF): $\tilde{\nu}/\text{cm}^{-1}$ 1978vs (CO), 1785s (μ -CO), 1590m (μ -CN). ¹H NMR (acetone-*d*₆): δ/ppm 9.44 (br-s, 1H, OH);

Chart 2. Structure of the Cation of 11b^a

^aNumbering refers to C atoms.

7.57–7.34 (m, 10H), 7.30–7.19 (m, 1H, C6–H), 7.03–6.92 (m, 1H, C8–H), 6.82–6.65 (m, 2H, C7–H + C9–H); 5.21, 5.00 (s, 5H/5H, Cp); 4.28, 4.21 (s, 3H/3H, NMe₂). ¹³C{¹H} NMR (acetone-*d*₆): δ/ppm 326.5 (d, ²J_{CP} = 17 Hz, μ-CN), 265.8 (d, ²J_{CP} = 14 Hz, μ-CO), 211.8 (d, ³J_{CP} = 2 Hz, CO), 158.9 (C10), 137.4 (d, ¹J_{CP} = 43 Hz, C5), 134.4 (d, ²J_{CP} = 6 Hz, C6), 133.3 (d, ²J_{CP} = 9 Hz, C2), 133.2 (d, ¹J_{CP} = 42 Hz, C1 + C1'), 132.8–132.4 (m, C2' + C8), 130.4; 130.0 (C4 + C4'); 128.3 (app. t, ³J_{CP} = 10 Hz, C3 + C3'), 123.0 (C7), 119.6 (d, ³J_{CP} = 9 Hz, C9); 89.7, 88.3 (Cp); 55.3, 51.7 (NMe₂). ³¹P{¹H} NMR (acetone-*d*₆): δ/ppm 51.2.

[Fe₂Cp₂(CO)(μ-CO){μ-η¹:η¹-CNMeXyl}(κ⁵-DMSO)]CF₃SO₃ (5b⁵). A bright red solution of 5b (64 mg, 0.10 mmol) and Me₃NO-

Chart 3. Structure of the Cation of 5b⁵

2H₂O (21 mg, 0.19 mmol) in DMSO/water 2/1 v/v (2 mL) was stirred at room temperature for 2 h. The resulting dark red solution was diluted with water (15 mL) and extracted with CH₂Cl₂ (3 × 15 mL). The organic phase was filtered over Celite and then dried under vacuum, affording a brown solid. Yield: 53 mg, 77%. Compound 5b⁵ is soluble in DMSO, acetone, and CH₂Cl₂, less soluble in CHCl₃, and insoluble in Et₂O. IR (solid state): $\tilde{\nu}/\text{cm}^{-1}$ 3104w, 2963w, 2924w, 2860w, 2119w, 2004s (CO), 1788s (μ-CO), 1516m (μ-CN), 1471w, 1421w, 1380m, 1319w, 1260s, 1223w, 1155s, 1107s (SO), 1084m-sh, 1029s, 1014s, 929w, 914w, 892w, 860m, 842m, 805m, 769s, 732m. IR (CH₂Cl₂): $\tilde{\nu}/\text{cm}^{-1}$ 2006s (CO), 1807s (μ-CO), 1521m (μ-CN). ¹H NMR (CDCl₃): δ/ppm 7.43–7.27 (m, 3H, C₆H₃Me₂), 5.12 (s, 5H, Cp), 4.69 (s, 3H, NCH₃), 4.58 (s, 5H, Cp), 3.36 (s, 3H, SCH₃), 3.14 (s, 3H, SCH₃), 2.67 (s, 3H, C₆H₃Me₂), 2.21 (s, 3H, C₆H₃Me₂). Slightly broadened resonances for CDCl₃ solutions were generally observed. ¹H NMR (acetone-*d*₆): δ/ppm 7.44–7.39 (m, 2H, C₆H₃), 7.37–7.34 (m, 1H, C₆H₃), 5.36 (s, 5H, Cp), 4.83 (s, 8H, Cp + NMe), 3.47 (s, 3H, SMe), 3.21 (s, 3H, SMe), 2.78 (s, 3H, CMe), 2.25 (s, 3H, CMe). ¹³C{¹H} NMR (acetone-*d*₆): δ/ppm 267.1 (μ-CO), 212.0 (CO); 134.9, 134.2, 132.2, 131.2, 130.0, 129.7 (C₆H₃); 90.2, 89.4 (Cp); 55.3, 53.9, 50.1 (SMe₂ + NMe); 19.0, 17.8 (CMe).

X-ray Crystallography. Crystal data and collection details for 11a^{Cl}·CH₃OH are reported in Table S2. Data were recorded on a Bruker APEX II diffractometer equipped with a PHOTON100 detector using Mo K α radiation and corrected for Lorentz-polarization and absorption effects (empirical absorption correction SADABS).⁵¹ The structure was solved by direct methods and refined by full-matrix least squares on the basis of all data using F².⁵² Hydrogen atoms were fixed at calculated positions and refined by a

riding model. All non-hydrogen atoms were refined with anisotropic displacement parameters.

Solubility in Water. A suspension of the selected Fe compound (3–5 mg) in a D₂O solution (1.0 mL) containing Me₂SO₂ as internal standard⁵³ (3.36 × 10⁻³ M) was vigorously stirred at 21 °C for 14 h. The resulting saturated solution was filtered over Celite, transferred into an NMR tube, and analyzed by ¹H NMR spectroscopy (delay time 3 s; number of scans 20). The concentration (=solubility) was calculated by the relative integral with respect to Me₂SO₂ (δ/ppm 3.14 (s, 6H)). Results are compiled in Table 1.

Octanol/Water Partition Coefficients (log P_{ow}). Partition coefficients (P_{ow}; IUPAC, K_D partition constant,⁵⁴ defined as P_{ow} = c_{org}/c_{aq} where c_{org} and c_{aq} are molar concentrations of the selected compound in the organic and aqueous phases, respectively) were determined by the shake-flask method and UV-vis measurements.⁵⁵ Deionized water and 1-octanol were vigorously stirred for 24 h, to allow saturation of both phases, and then separated by centrifugation. A stock solution of the selected Fe compound (ca. 2 mg) was prepared by first adding CH₂Cl₂ (25 μL, to help solubilization), followed by water-saturated octanol (4 mL) and vigorous stirring at room temperature for 30 min or until complete dissolution. The solution was diluted with water-saturated octanol (ca. 1/4 v/v ratio, c_{Fe} ≈ 10⁻⁴ M, so that 1.0 ≤ A ≤ 1.5 at λ_{max}) and its UV-vis spectrum was recorded (A⁰_{org}). An aliquot of the solution (V_{org} = 1.5 mL) was transferred into a test tube, and octanol-saturated water (V_{org} = V_{aq} = 1.5 mL) was added. The mixture was vigorously stirred for 30 min at 21 °C and then centrifuged (5000 rpm, 10 min). The UV-vis spectrum of the organic phase was recorded (A^f_{org}), and the partition coefficient was calculated as P_{ow} = A^f_{org}/(A⁰_{org} - A^f_{org}), where A⁰_{org} and A^f_{org} are the absorbances in the organic phase before and after partition with the aqueous phase, respectively.^{55c} For compound 5a, the initial solution was prepared in octanol-saturated water, following an inverse procedure, and the partition coefficient was calculated as P_{ow} = (A⁰_{aq} - A^f_{aq})/A^f_{aq}, where A⁰_{aq} and A^f_{aq} are the absorbances in the aqueous phase before and after partition with the organic phase, respectively. UV-vis spectra were recorded using PMMA cuvettes (1 cm path length) in the 250–800 nm range. The wavelength of the maximum absorption of each compound (320–390 nm range) was used for UV-vis quantitation. The procedure was repeated three times for each sample (from the same stock solution); results are given as mean ± standard deviation (Table 1).

Stability in Aqueous Solutions. Stability in H₂O. A mixture of the selected Fe compound (3, 4, 5a–c, 11a; ca. 4 mg) and a D₂O solution (0.9 mL) containing Me₂SO₂ (3.36 × 10⁻³ M) was stirred for 30 min and then filtered over Celite and transferred into an NMR tube. The orange-red (3, 4, 5a–c) or dark green (11a) solutions were analyzed by ¹H, ¹⁹F, and ³¹P{¹H} NMR and then heated at 37 °C for 72 h. After it was cooled to room temperature, the final solution was separated from an orange-brown solid by filtration over Celite and NMR analyses were repeated. The amount of starting material in solution (percent with respect to the initial spectrum) was calculated by the relative integral with respect to Me₂SO₂ as an internal standard⁵³ (δ/ppm 3.14 (s, 6H)) (Table S3). The aqueous solution was then extracted with CDCl₃ (3 × 0.25 mL) and analyzed by ¹H and ¹⁹F NMR, in order to confirm the identity of the compounds. NMR data for the tested compounds are given in the Supporting Information.

Isolation and Identification of the Precipitate from H₂O. A suspension of 5a (82 mg) in H₂O (20 mL) was vigorously stirred at room temperature for 30 min and then filtered over Celite. The resulting red solution was stirred at 37 °C for 72 h and then cooled to room temperature and filtered (G4 porous filter). The resulting brown solid was washed with water and dried under vacuum (40 °C). Yield: 22 mg. The sample was analyzed by Raman spectroscopy and identified as hematite (Raman shifts: 698br cm⁻¹). IR (solid state) also indicated the presence of water in the sample (3400–3200 cm⁻¹). An analogous experiment was carried out using 5b (33 mg), yielding a brown solid (13 mg) identified as a mixture of hematite (Raman shifts: 218, 283, 398, 491, 599 cm⁻¹) and magnetite (Raman

shifts: 683br cm^{-1}). IR (solid state) also indicated the presence of water in the sample ($3400\text{--}3200\text{ cm}^{-1}$).

Stability in DMSO/Water. A mixture of the selected compound (**5d**, **6**, **7**, **9**, **10**, **11b**; ca. 4 mg), DMSO- d_6 (0.6 mL), and a D₂O solution (0.3 mL; 0.2 mL for **7** and **9a**) containing Me₂SO₂ ($3.36 \times 10^{-3}\text{ M}$) was stirred for 30 min and then filtered over Celite and transferred into an NMR tube. The resulting orange-red (**5d**, **e**, **10**), yellow-brown (**6**, **7**, **9a**), or dark green (**9b**, **11b**) solution was analyzed by ¹H, ¹⁹F, and ³¹P{¹H} NMR and then heated at 37 °C for 72 h. After it was cooled to room temperature, the solution was filtered over Celite and NMR analyses were repeated. The amount of starting material in solution (percent with respect to the initial spectrum) was calculated by the relative integral with respect to Me₂SO₂ as an internal standard⁵³ (δ/ppm 2.95 (s, 6H)) (Table S4). NMR data for the tested compounds are given in the Supporting Information; ¹H chemical shifts are referenced to the DMSO- d_5 signal as in pure DMSO- d_6 (δ/ppm 2.50).

Reference Data for [Fe₂Cp₂(CO)(μ -CO){ μ -CN(Me)R}(DMSO)]CF₃SO₃ species (5^s**).** A mixture of **5a–e** (ca. 7 mg) and Me₃NO \cdot 2H₂O (1.5 equiv) in DMSO- d_6 /D₂O 2/1 v/v (0.9 mL) was filtered over Celite and transferred into an NMR tube. The red-brown solution was maintained at room temperature for 1–4 h and periodically analyzed by ¹H NMR. The progressive formation of [Fe₂Cp₂(CO)(μ -CO){ μ -CN(Me)R}(DMSO)]CF₃SO₃ (**5^s**) was observed; NMR data are reported below. [Fe₂Cp₂(CO)(μ -CO){ μ -CNMe₂}(DMSO)]CF₃SO₃ (**5a^s**): ¹H NMR (DMSO- d_6 /D₂O 2/1) δ/ppm 5.15 (s, 5H), 4.97 (s, 5H), 4.32 (s, 3H), 4.04 (s, 3H). [Fe₂Cp₂(CO)(μ -CO){ μ -CN(Me)Xyl}(DMSO)]CF₃SO₃ (**5b^s**): ¹H NMR (DMSO- d_6 /D₂O 2/1) δ/ppm 7.45–7.30 (m, 2H), 7.29–7.23 (m, 1H); 5.34, 5.11 (s, 5H); 4.66, 4.64 (s, 5H); 4.54 (s, 2.5H), 2.61, 2.56 (s, 3H); 2.07, 2.05 (s, 3H). Isomer ratio 4/1. [Fe₂Cp₂(CO)(μ -CO){ μ -CN(Me)Naph}(DMSO)]CF₃SO₃ (**5d^s**): ¹H NMR (DMSO- d_6 /D₂O 2/1) δ/ppm 8.32–7.85 (m, 5H), 7.74–7.54 (m, 3H); 5.31, 5.13 (s, 5H), 4.75, 4.46 (s, 3H); 4.56, 4.52 (s, 5H). Isomer ratio 4:1. [Fe₂Cp₂(CO)(μ -CO){ μ -CN(Me)Xyl^{Cl}}(DMSO)]CF₃SO₃ (**5e^s**): ¹H NMR (DMSO- d_6 /D₂O 2/1) δ/ppm 7.62–7.42 (m, 3H); 5.38, 5.34, 5.19, 5.13 (s, 5H); 4.75, 4.72, 4.70, 4.65, 4.58, 4.56, 4.50, 4.40 (s, 8H); 2.67, 2.63, 2.17, 2.14 (s, 3H). Isomer ratio ca. 3:2:1:1.

Stability in Cell Culture Medium. The selected Fe compound (ca. 6 mg) was dissolved in DMSO (0.1 mL for **4**, **5a–c**, **cis-11a**; 1.0 mL for **5d**, **e**, **6**, **9b**, **11b**; 2.0 mL for **9a**, **10**) and then diluted with RPMI-1640 cell culture medium (Merck; modified with sodium bicarbonate, without L-glutamine and phenol red) up to 5.0 mL. The red-orange (**4**, **5a–e**, **10**), yellow-brown (**6**, **9a**) or dark green (**9b**, **11a**, **b**) solution was heated at 37 °C for 72 h and then cooled to room temperature. The resulting suspension was diluted with water (5 mL) and extracted with CH₂Cl₂ ($3 \times 10\text{ mL}$). The combined organic extracts were dried under vacuum (40 °C), and the residue was analyzed by IR (CH₂Cl₂) and ¹H and ³¹P{¹H} NMR (CDCl₃; acetone- d_6 for **11a**). In all cases the starting material was identified; IR data are reported in the Supporting Information.

CO Release. In 5 mL test tubes equipped with rubber septa, suspensions of **5b** and **9a** (ca. 10 mg) in RPMI-1640 cell culture medium (4 mL) were heated at 37 °C. After 24 h, the headspace was sampled with a 500 μL gastight microsyringe and analyzed by GC-TCD. A peak ascribable to carbon monoxide in the chromatogram was identified in both cases and confirmed by the analysis on a pure CO sample.

Cytotoxicity. Reagents. Dulbecco's Modified Eagle Medium (DMEM), Roswell Park Memorial Institute (RPMI) 1640 medium, trypsin 0.05%/EDTA 1X solution, penicillin 10,000 U/mL, streptomycin 10 mg/mL solution, L-glutamine 200 mM, nonessential amino acid solution 100X, fetal calf serum (FCS), plates, and Petri dishes were purchased from EuroClone. The compounds were dissolved in DMSO, while cisplatin (Merck) was dissolved in bidistilled ultrapure water before performing each experiment. The maximum analyzed concentration of Fe compounds was 200 μM , while cisplatin was tested up to 100 μM . The amount of DMSO did not exceed the culture media volume by 0.25%.

Cell Culture. MDA-MB-231 and SMC cells were cultured in DMEM, whereas A2780 cells were cultured in RPMI-1640. Both of the culture media were supplemented with 10% FCS, 1% nonessential amino acids 100X, 1% penicillin/streptomycin solution, and 1% L-glutamine 200 mM at 37 °C, under a humidified atmosphere (5% CO₂ and 95% air).

Cell Viability Assay. A sulforhodamine B (SRB) assay was performed to assess the cell viability after treatments. A total of 8000 cells/well was seeded in a 96-well tray in triplicate. After 24 h of incubation, the cells were treated with different concentrations of compounds. SRB assays were performed after 48 h as previously described.⁵⁶

RT-qPCR Analysis. Reverse transcription (RT) followed by a quantitative polymerase chain reaction (qPCR) was used to evaluate the effect of **5b** (5 and 10 μM) and **9b** (25 and 50 μM) on p53 mRNA levels (Figure 3) in the A2780 cell line. A total of 80000 cells/well was seeded into a 48-well tray in complete medium and incubated the day after with indicated concentrations of the complexes. After 24 h, mRNA was isolated (iScript, Bio-Rad) and reverse-transcribed (Maxima First Strand cDNA Synthesis Kit, Thermo Scientific). p53 and 18S mRNA levels were amplified and quantified (ExcelTaq 2X Q-PCR Master Mix, SMO-BIO). 18S values were used to normalize the results.

Statistical Analysis. Experimental data are expressed as mean \pm SD. The effects of the complexes versus control were analyzed by a two-tailed Student's *t* test for unpaired data. The concentration of compounds required to reduce the cell viability by 50% (IC₅₀) was calculated using a nonlinear regression curve (GraphPad Prism, Version 5.01).

Quantification of Iron Cellular Uptake. The determination of total intracellular iron amount was carried out on MDA-MB-231 cells by seeding 500000 cells/well into a six well-tray in complete medium. After 1 day, the cells were incubated during 24 h with the complexes at different levels of concentration (Table 3). The experiments were performed in triplicate. At the end of the incubation, cell monolayers were washed twice with PBS and lysed by incubation with a homemade lysis buffer (50 mM TRIS pH 7.5, 150 mM NaCl, 0.5% v/v Nonidet P40, protease and phosphatase inhibitors, in bidistilled ultrapure water), during 30 min on ice. Cell lysates were then cleared by centrifugation during 10 min at 4 °C; the total amount of protein was thus quantified with a BCA assay kit by EuroClone following the manufacturer instructions.

An Agilent Model 7700 quadrupole ICP-MS (Agilent Technologies, Tokyo, Japan) equipped with a collision cell system and an Agilent Model ASX-520 autosampler (Agilent Technologies, Tokyo, Japan) were used for sample analysis. The instrument was fitted with a MicroMist nebulizer (Agilent nebulizer standard for 7700) with a Scott-type double-pass glass spray chamber cooled to 4 °C. A solution of 20 $\mu\text{g/L}$ of iridium in 2% HNO₃ was used as an internal standard (207209, Merck). Iron standard solutions were prepared in 2% HNO₃ from a standard (iron atomic spectroscopy standard concentrate 10.00 mg/L Fe). The final calibration range was 5–100 $\mu\text{g/L}$. Iron was quantified on the *m/z* 56 (⁵⁶Fe) isotope. Each sample was diluted just before the analysis in 2.3 mL of 2% HNO₃. Samples and standards were analyzed in triplicate. Sample blanks and standard solutions were run with each batch of samples as quality control. The method was validated by the analysis of certified reference material SRM 1643f (Trace Elements in Water, National Institute of Standards and Technology; nominal Fe concentration $93.4 \pm 0.8\text{ }\mu\text{g/L}$, determined Fe concentration $92.1 \pm 0.7\text{ }\mu\text{g/L}$) and recovery experiments on the internal standard (iridium; average recovery $100 \pm 6\%$). Fe concentrations were normalized with respect to the protein content determined by using the BCA protein assay (Thermo Scientific, Rockford, IL, USA) ($10^{-8}\text{ g Fe/mg protein}$) and expressed as mean \pm standard deviation of the three independent samples for each condition (Table 3). The Fe content in untreated cells ($16 \pm 3 \times 10^{-8}\text{ g Fe/mg protein}$) was comparable to previously reported data (different cell lines).⁵⁷

Determination of the Intracellular Levels of Reactive Oxygen Species (ROS). The intracellular levels of reactive oxygen

species (ROS) upon treatment with the analyzed complexes was measured by using the H₂-DCF-DA (2',7'-dichlorodihydrofluorescein diacetate; Merck) assay. Upon cleavage of the acetate groups by intracellular esterase and oxidation, H₂-DCF-DA is converted to the fluorescent 2',7'-dichlorofluorescein (DCF). Briefly, MDA-MB-231 cells were seeded at concentration of 8000 cells/well in complete growth medium into 96-well black plates. After overnight incubation, cells were incubated for 24 h with different concentrations of complexes. At the end of the incubation, the culture medium was removed and the cells were washed twice with PBS and incubated with H₂-DCF-DA 10 μM dissolved in Hanks' Balanced Salt Solution (HBSS) for 30 min, in the dark at 37 °C. The fluorogenic probe solution was thus removed, and the cells were washed with PBS. After addition of 100 μL/well of PSA, the DCF fluorescence intensity was immediately measured at excitation 485 nm/emission 535 nm, using a Multilabel Plate Reader VICTOR Nivo (PerkinElmer). The fold increase in ROS production was calculated using the equation $(F_{\text{treatment}} - F_{\text{blank}})/(F_{\text{control}} - F_{\text{blank}})$, where F is the fluorescence reading.

Catalytic NADH Oxidation. NADH was stored at -20 °C under N₂; a stock NADH solution (2.3×10^{-4} M) was prepared in phosphate-buffered aqueous solution (Na₂HPO₄/NaH₂PO₄; 5.4×10^{-3} M, pH 7.28) and stored at 4 °C. Stock solutions of selected Fe compounds (**5a**, **b**, **d** and **9a**, **b**; 2.0×10^{-4} M) were prepared in MeOH immediately before use; FeSO₄ was dissolved in a small amount of H₂O and then diluted in MeOH. Solutions of each Fe compound (0.35 mL) and NADH (6.5 mL) were mixed, resulting in a 95/5 v/v H₂O/MeOH solution containing 2.2×10^{-4} M NADH and 1.0×10^{-5} M Fe compound (4.5 mol %). The solution was stirred at 37 °C for 26 h and periodically analyzed by UV-vis spectroscopy (260–460 nm) using PMMA cuvettes (1.0 cm path length). Turnover numbers were calculated as $\text{TON} = c(0)/c_{\text{Fe}} \times [A(0) - A(t)]/A(0)$, where A is the absorbance at $\lambda_{\text{max}} = 339$ nm; $c(0)$ and c_{Fe} are the initial molar concentrations of NADH and the selected Fe compound, respectively (Table 4).

Interaction of 5b with Biomolecules. Fluorescence measurements were performed on a PerkinElmer LS55 instrument with temperature control to within ± 0.1 °C. Calf thymus DNA (highly polymerized sodium salt, abbreviated as DNA in the text) and ethidium bromide (EB, purity >98%) were purchased from Merck. DNA was sonicated to reduce its length to ca. 500 base pairs following a published procedure.⁵⁸ The concentrations of DNA (C_{DNA} , $\epsilon_{260\text{ nm}} = 13200 \text{ M}^{-1} \text{ cm}^{-1}$ for molar concentrations in base pairs), EB (C_{EB} , $\epsilon_{480\text{ nm}} = 5700 \text{ M}^{-1} \text{ cm}^{-1}$), and BSA (C_{BSA} , $\epsilon_{278\text{ nm}} = 44000 \text{ M}^{-1} \text{ cm}^{-1}$) were spectrophotometrically determined. Solutions of the metal complex were prepared by weighing appropriate amounts of the solid and dissolving it into DMSO (1.29×10^{-3} M stock solution). Ultrapure water (Sartorius) was the reaction medium together with a NaCl 0.1 M + NaCac (sodium cacodylate) aqueous buffer used to maintain pH 7.0. In EB/DNA exchange experiments, DNA was saturated with EB according to a known procedure;⁵⁹ in brief, EB was added to DNA until the fluorescence emission increase at the excitation/emission wavelength selective for the EB/DNA intercalated complex faded out ($T = 25.0$ °C, $C_{\text{DNA}} = 1.30 \times 10^{-4}$ M, $C_{\text{EB}} = 5.33 \times 10^{-5}$ M, $C_{\text{DNA}}/C_{\text{EB}} = 2.4$, $\lambda_{\text{ex}} = 520$ nm, $\lambda_{\text{em}} = 595$ nm). Subsequently, increasing amounts of the stock metal complex solution were added to the EB/DNA mixture (Figure S1). Additions of the concentrated titrant were carried out with a gastight syringe connected to a Mitutoyo micrometric screw (minimum addition possible 0.164 μL). The additions were such that DMSO < 7.5% and the absorbance of **5b** at 280 nm was <0.05 (to avoid inner filter bias). A blank test was carried out by adding DMSO to the EB/DNA mixture, in order to quantify fluorescence changes due to dilution/solvent effects. In the case of **5b**/BSA fluorescence titrations (Figure S2A), the analyzed metal complex (6.14×10^{-5} M) was added to a 3.14×10^{-7} M BSA solution ($\lambda_{\text{ex}} = 280$ nm, $\lambda_{\text{em}} = 345$ nm). The volumes of the added solutions of **5b** were small enough to ensure a negligible presence of DMSO in the system.

■ ASSOCIATED CONTENT

Supporting Information

The Supporting Information is available free of charge at <https://pubs.acs.org/doi/10.1021/acs.organomet.9b00681>.

X-ray data, stability studies, details of binding studies with biomolecules, and NMR spectra of new compounds (PDF)

Accession Codes

CCDC 1955487 contains the supplementary crystallographic data for this paper. These data can be obtained free of charge via www.ccdc.cam.ac.uk/data_request/cif, or by emailing data_request@ccdc.cam.ac.uk, or by contacting The Cambridge Crystallographic Data Centre, 12 Union Road, Cambridge CB2 1EZ, UK; fax: +44 1223 336033.

■ AUTHOR INFORMATION

Corresponding Authors

Nicola Ferri – Dipartimento di Scienze del Farmaco, Università degli Studi di Padova, 35131 Padova, Italy;

Email: nicola.ferri@unipd.it

Valerio Zanotti – Dipartimento di Chimica Industriale “Toso Montanari”, Università di Bologna, I-40136 Bologna, Italy;

orcid.org/0000-0003-4190-7218; Email: valerio.zanotti@unibo.it

Fabio Marchetti – Dipartimento di Chimica e Chimica Industriale, Università di Pisa, I-56124 Pisa, Italy;

orcid.org/0000-0002-3683-8708;

Email: fabio.marchetti1974@unipi.it; https://people.unipi.it/fabio_marchetti1974/

Authors

Gabriele Agonigi – Dipartimento di Chimica e Chimica Industriale, Università di Pisa, I-56124 Pisa, Italy

Lorenzo Biancalana – Dipartimento di Chimica e Chimica Industriale, Università di Pisa, I-56124 Pisa, Italy

Maria Giovanna Lupo – Dipartimento di Scienze del Farmaco, Università degli Studi di Padova, 35131 Padova, Italy

Monica Montopoli – Dipartimento di Scienze del Farmaco, Università degli Studi di Padova, 35131 Padova, Italy

Stefano Zacchini – Dipartimento di Chimica Industriale “Toso Montanari”, Università di Bologna, I-40136 Bologna, Italy;

orcid.org/0000-0003-0739-0518

Francesca Binacchi – Dipartimento di Chimica e Chimica Industriale, Università di Pisa, I-56124 Pisa, Italy

Tarita Biver – Dipartimento di Farmacia and Dipartimento di Chimica e Chimica Industriale, Università di Pisa, I-56126 Pisa, Italy; orcid.org/0000-0001-8512-8422

Beatrice Campanella – Istituto di Chimica dei Composti Organometallici, Consiglio Nazionale delle Ricerche, I-56124 Pisa, Italy

Guido Pampaloni – Dipartimento di Chimica e Chimica Industriale, Università di Pisa, I-56124 Pisa, Italy;

orcid.org/0000-0002-6375-4411

Complete contact information is available at:

<https://pubs.acs.org/doi/10.1021/acs.organomet.9b00681>

Author Contributions

*G.A., L.B., and M.G.L. contributed equally to this work.

Notes

The authors declare no competing financial interest.

ACKNOWLEDGMENTS

We gratefully thank the University of Pisa for financial support (PRA_2017_25, "composti di metalli di transizione come possibili agenti antitumorali").

REFERENCES

- (1) Selected references: (a) Natinsky, B. S.; Liu, C. Two are better than one. *Nat. Chem.* **2019**, *11*, 200–201. (b) Huang, G. H.; Li, J.-M.; Huang, J.-J.; Lin, J.-D.; Chuang, G. J. Cooperative Effect of Two Metals: CoPd(OAc)₄-Catalyzed C-H Amination and Aziridination. *Chem. - Eur. J.* **2014**, *20*, 5240–5243. (c) Cooper, O.; Camp, C.; Pecaut, J.; Kefalidis, C. E.; Maron, L.; Gambarelli, S.; Mazzanti, M. Multimetallic Cooperativity in Uranium-Mediated CO₂ Activation. *J. Am. Chem. Soc.* **2014**, *136*, 6716–6723. (d) Ritleng, V.; Chetcuti, M. J. Hydrocarbyl Ligand Transformations on Heterobimetallic Complexes. *Chem. Rev.* **2007**, *107*, 797–858.
- (2) (a) Mazzoni, R.; Marchetti, F.; Cingolani, A.; Zanotti, V. Bond Forming Reactions Involving Isocyanides at Diiron Complexes. *Inorganics* **2019**, *7*, 25. (b) Marchetti, F. Constructing Organometallic Architectures from Aminoalkylidyne Diiron Complexes. *Eur. J. Inorg. Chem.* **2018**, *2018*, 3987–4003. (c) Mazzoni, R.; Salmi, M.; Zanotti, V. C-C Bond Formation in Diiron Complexes. *Chem. - Eur. J.* **2012**, *18*, 10174–10194.
- (3) (a) Bauer, I.; Knolker, H. J. Iron Catalysis in Organic Synthesis. *Chem. Rev.* **2015**, *115*, 3170–3387. (b) Bleith, T.; Wadepohl, H.; Gade, L. H. Iron Achieves Noble Metal Reactivity and Selectivity: Highly Reactive and Enantioselective Iron Complexes as Catalysts in the Hydrosilylation of Ketones. *J. Am. Chem. Soc.* **2015**, *137*, 2456–2459. (c) Chirik, P. J. In *Catalysis Without Precious Metals*; Bullock, R. M., Ed.; Wiley-VCH: Weinheim, 2010; pp 83–110. (d) Fürstner, A. Iron Catalysis in Organic Synthesis: A Critical Assessment of What It Takes To Make This Base Metal a Multitasking Champion. *ACS Cent. Sci.* **2016**, *2*, 778–789. (e) Piontek, A.; Bisz, E.; Szostak, M. Iron-Catalyzed Cross-Couplings in the Synthesis of Pharmaceuticals: In Pursuit of Sustainability. *Angew. Chem., Int. Ed.* **2018**, *57*, 11116–11128.
- (4) (a) Schilter, D.; Camara, J. M.; Huynh, M. T.; Hammes-Schiffer, S.; Rauchfuss, T. B. Hydrogenase enzymes and their synthetic models: the role of metal hydrides. *Chem. Rev.* **2016**, *116*, 8693–8749. (b) Capon, J. F.; Gloaguen, F.; Pétilion, F. Y.; Schollhammer, P.; Talarmin, J. Electron and proton transfers at diiron dithiolate sites relevant to the catalysis of proton reduction by the [FeFe]-hydrogenases. *Coord. Chem. Rev.* **2009**, *253*, 1476–1494. (c) Gloaguen, F. Electrochemistry of simple organometallic models of iron-iron hydrogenases in organic solvent and water. *Inorg. Chem.* **2016**, *55*, 390–398. (d) Cheah, M. H.; Tard, C.; Borg, S. J.; Liu, X.; Ibrahim, S. K.; Pickett, C. J.; Best, S. P. Modeling [Fe–Fe] hydrogenase: evidence for bridging carbonyl and distal iron coordination vacancy in an electrocatalytically competent proton reduction by an iron thiolate assembly that operates through Fe(0)–Fe(II) levels. *J. Am. Chem. Soc.* **2007**, *129*, 11085–11092. (e) Harb, M. K.; Apfel, U. P.; Kubel, J.; Górs, H.; Felton, G. A. N.; Sakamoto, T.; Evans, D. H.; Glass, R. S.; Lichtenberger, D. L.; El-Khateeb, M.; Weigand, W. Preparation and characterization of homologous diiron dithiolato, diselenato, and ditellurato complexes: [FeFe]-hydrogenase models. *Organometallics* **2009**, *28*, 6666–6675.
- (5) Li, Y.; Rauchfuss, T. B. Synthesis of diiron(I) dithiolato carbonyl complexes. *Chem. Rev.* **2016**, *116*, 7043–7077.
- (6) (a) Mazzoni, R.; Gabiccini, A.; Cesari, C.; Zanotti, V.; Gualandi, I.; Tonelli, D. Diiron complexes bearing bridging hydrocarbyl ligands as electrocatalysts for proton reduction. *Organometallics* **2015**, *34*, 3228–3235. (b) Arrigoni, F.; Bertini, L.; De Gioia, L.; Cingolani, R.; Mazzoni, R.; Zanotti, V.; Zampella, G. Mechanistic Insight into Electrocatalytic H₂ Production by [Fe₂(CN){μ-CN(Me)₂}(μ-CO)(CO)(Cp)₂]: Effects of Dithiolate Replacement in [FeFe] Hydrogenase Models. *Inorg. Chem.* **2017**, *56*, 13852–13864.
- (7) (a) Zanotti, V. Reactions of bridging C₃ ligands in diiron complexes: Unconventional routes to new functionalized organic frames. *Pure Appl. Chem.* **2010**, *82*, 1555–1568. (b) Marchetti, F.; Zacchini, S.; Zanotti, V. Growing the Molecular Architecture at Alkynyl(amino)carbene Ligands in Diiron μ-Aminocarbene Complexes. *Eur. J. Inorg. Chem.* **2016**, *2016*, 4820–4828. (c) Marchetti, F.; Zacchini, S.; Zanotti, V. Photochemical Alkyne Insertions into the Iron–Thiocarbonyl Bond of [Fe₂(CS)(CO)₃(Cp)₂]. *Organometallics* **2016**, *35*, 2630–2637. (d) Boni, A.; Funaioli, T.; Marchetti, F.; Pampaloni, G.; Pinzino, C.; Zacchini, S. Reversible Reductive Dimerization of Diiron μ-Vinyl Complex via C–C Coupling: Characterization and Reactivity of the Intermediate Radical Species. *Organometallics* **2011**, *30*, 4115–4122.
- (8) (a) Patra, M.; Gasser, G. The medicinal chemistry of ferrocene and its derivatives. *Nat. Rev.* **2017**, *1*, 1–11. (b) Ali Larik, F.; Saeed, A.; Fattah, T. A.; Muqadar, U.; Channar, P. A. Recent advances in the synthesis, biological activities and various applications of ferrocene derivatives. *Appl. Organomet. Chem.* **2017**, *31*, e3664.
- (9) (a) Held, J.; Supan, C.; Salazar, C. L. O.; Tinto, H.; Bonkian, L. N.; Nahum, A.; Moulero, B.; Sié, A.; Coulibaly, B.; Sirima, S. B.; Siribie, M.; Otsyula, N.; Otieno, L.; Abdallah, A. M.; Kimutai, R.; Bouyou-Akotet, M.; Kombila, M.; Koiwai, K.; Cantalloube, C.; Din-Bell, C.; Djeriou, E.; Waitumbi, J.; Mordmüller, B.; Ter-Minassian, D.; Lell, B.; Kremsner, P. G. Ferroquine and artesunate in African adults and children with Plasmodium falciparum malaria: a phase 2, multicentre, randomised, double-blind, dose-ranging, non-inferiority study. *Lancet Infect. Dis.* **2015**, *15*, 1409–1419. (b) McCarthy, J. S.; Rückle, T.; Djeriou, E.; Cantalloube, C.; Ter-Minassian, D.; Baker, M.; O'Rourke, P.; Griffin, P.; Marquart, L.; van Huijsduijnen, R. H.; Möhrle, J. J. A Phase II pilot trial to evaluate safety and efficacy of ferroquine against early Plasmodium falciparum in an induced blood-stage malaria infection study. *Malar. J.* **2016**, *15*, 496.
- (10) Kondratskyi, A.; Kondratska, K.; Vanden Abeele, F.; Gordienko, D.; Dubois, C.; Toillon, R.-A.; Slomianny, C.; Lemière, S.; Delcourt, P.; Dewailly, E.; Skryma, R.; Biot, C.; Prevarskaya, N. Ferroquine, the next generation antimalarial drug, has antitumor activity. *Sci. Rep.* **2017**, *7*, 15896.
- (11) (a) Jaouen, G.; Vessieres, A.; Top, S. Ferrocifen type anti cancer drugs. *Chem. Soc. Rev.* **2015**, *44*, 8802–8817. (b) Wang, Y.; Dansette, P. M.; Pigeon, P.; Top, S.; McGlinchey, M. J.; Mansuy, D.; Jaouen, G. A new generation of ferrociphenols leads to a great diversity of reactive metabolites, and exhibits remarkable antiproliferative properties. *Chem. Sci.* **2018**, *9*, 70–78.
- (12) Rocco, D.; Batchelor, L. K.; Agonigi, G.; Braccini, S.; Chiellini, F.; Schoch, S.; Biver, T.; Funaioli, T.; Zacchini, S.; Biancalana, L.; Ruggeri, M.; Pampaloni, G.; Dyson, P. J.; Marchetti, F. Anticancer Potential of Diiron Vinyliminium Complexes. *Chem. - Eur. J.* **2019**, *25*, 14801–14816.
- (13) (a) Dyke, A. F.; Knox, S. A. R.; Naish, P. J.; Taylor, G. E. Organic chemistry of dinuclear metal centres. Part 1. Combination of alkynes with carbon monoxide at di-iron and diruthenium centres: crystal structure of [Ru₂(CO)(μ-CO){μ-σ-η³-C(O)C₂Ph₂}(η-C₅H₅)₂]. *J. Chem. Soc., Dalton Trans.* **1982**, 1297–1307. (b) Boni, A.; Funaioli, T.; Marchetti, F.; Pampaloni, G.; Pinzino, C.; Zacchini, S. Electrochemical, EPR and Computational Results on [Fe₂Cp₂(CO)₂]-Based Complexes with a Bridging Hydrocarbyl Ligand. *J. Organomet. Chem.* **2011**, *696*, 3551–3556.
- (14) (a) Boni, A.; Marchetti, F.; Pampaloni, G.; Zacchini, S. Cationic Diiron and Diruthenium μ-Allenyl Complexes: Synthesis, X-Ray Structures and Cyclization Reactions with Ethyldiazoacetate/Amine Affording Unprecedented Butenolide- and Furaniminium-Substituted Bridging Carbene Ligands. *Dalton Trans.* **2010**, *39*, 10866–10875. (b) Agonigi, G.; Bortoluzzi, M.; Funaioli, T.; Marchetti, F.; Pampaloni, G.; Zacchini, S. Synthesis of diiron μ-allenyl complexes by electrophilic addition to propen-2-yl-dimetallacyclopentenone species: A joint experimental and DFT study. *J. Organomet. Chem.* **2013**, *731*, 61–66.
- (15) (a) Wagner, R. E.; Jacobson, R. A.; Angelici, R. J.; Quick, M. H. Synthesis of thiocarbonyl-bridged(η⁵-C₅H₅)₂Fe₂(CO)₃(CS) and crystal structure of an s-alkylated derivative. *J. Organomet. Chem.* **1978**, *148*, C35–C39. (b) Schroeder, N. C.; Funchess, R.; Jacobson,

R. A.; Angelici, R. J. Reactions of $\text{Cp}_2\text{Fe}_2(\text{CO})_2(\mu\text{-CO})(\mu\text{-CSR})^+$ bridging-carbyne complexes with nucleophiles. *Organometallics* **1989**, *8*, 521–529.

(16) (a) Agonigi, G.; Bortoluzzi, M.; Marchetti, F.; Pampaloni, G.; Zacchini, S.; Zanotti, V. Regioselective Nucleophilic Additions to Diiron Carbonyl Complexes Containing a Bridging Aminocarbyne Ligand: A Synthetic, Crystallographic and DFT Study. *Eur. J. Inorg. Chem.* **2018**, *2018*, 960–971. (b) Albano, V. G.; Busetto, L.; Castellari, C.; Monari, M.; Palazzi, A.; Zanotti, V. Electrophilically promoted cyanide abstraction in diiron cyano(amino) alkylidene complexes: molecular structure of $[\text{Fe}_2(\text{CO})_2(\eta\text{-C}_5\text{H}_5)_2(\mu\text{-CO})\{\mu\text{-CN}(\text{CH}_2)_4\text{CH}_2\}][(\text{OC})_5\text{WCNW}(\text{CO})_5]$. *J. Chem. Soc., Dalton Trans.* **1993**, 3661–3666.

(17) Busetto, L.; Marchetti, F.; Zacchini, S.; Zanotti, V. *Inorg. Chim. Acta* **2005**, *358*, 1469–1484.

(18) Albano, V. G.; Busetto, L.; Marchetti, F.; Monari, M.; Zacchini, S.; Zanotti, V. Synthesis and Characterization of New Diiron and Diruthenium μ -Aminocarbyne Complexes Containing Terminal S-, P- and C-Ligands. *Z. Naturforsch., B: J. Chem. Sci.* **2007**, *62b*, 427–438.

(19) Albano, V. G.; Busetto, L.; Camiletti, C.; Castellari, C.; Monari, M.; Zanotti, V. Selective C–C bond formation at diiron μ -aminocarbyne complexes. *J. Chem. Soc., Dalton Trans.* **1997**, 4671–4676.

(20) Albano, V. G.; Busetto, L.; Monari, M.; Zanotti, V. Reactions of acetonitrile di-iron μ -aminocarbyne complexes; synthesis and structure of $[\text{Fe}_2(\mu\text{-CNMe}_2)(\mu\text{-H})(\text{CO})_2(\text{Cp})_2]$. *J. Organomet. Chem.* **2000**, *606*, 163–168.

(21) Marchetti, F.; Zacchini, S.; Zanotti, V. Coupling of Isocyanide and μ -Aminocarbyne Ligands in Diiron Complexes Promoted by Hydride Addition. *Organometallics* **2014**, *33*, 3990–3997.

(22) Examples of Pt complexes: (a) Živković, M. D.; Kljun, J.; Ilic-Tomic, T.; Pavic, A.; Veselinović, A.; Manojlović, A. A.; Nikodinovic-Runic, J.; Turel, I. A new class of platinum(II) complexes with the phosphine ligand pta which show potent anticancer activity. *Inorg. Chem. Front.* **2018**, *5*, 39–53. (b) Babak, M. V.; Pfaffeneder-Kmen, M.; Meier-Menches, S. M.; Legina, M. S.; Theiner, S.; Licon, C.; Orvain, C.; Hejl, M.; Hanif, M.; Jakupec, M. A.; Keppler, B. K.; Gaiddon, C.; Hartinger, C. G. Rollover Cyclometalated Bipyridine Platinum Complexes as Potent Anticancer Agents: Impact of the Ancillary Ligands on the Mode of Action. *Inorg. Chem.* **2018**, *57*, 2851–2864.

(23) Examples of Ru complexes: (a) Pettinari, R.; Condello, F.; Marchetti, F.; Pettinari, C.; Smoleński, P.; Riedel, T.; Scopelliti, R.; Dyson, P. J. Dicationic Ruthenium(II)–Arene–Curcumin Complexes Containing Methylated 1,3,5-Triaza-7-phosphaadamantane: Synthesis, Structure, and Cytotoxicity. *Eur. J. Inorg. Chem.* **2017**, *2017*, 2905–2910. (b) Wołoszyn, A.; Pettinari, C.; Pettinari, R.; Badillo Patzmay, G. V.; Kwiecień, A.; Lupidi, G.; Nabissi, M.; Santoni, G.; Smoleński, P. Ru(II)-(PTA) and -mPTA complexes with N2-donor ligands bipyridyl and phenanthroline and their antiproliferative activities on human multiple myeloma cell lines. *Dalton Trans.* **2017**, *46*, 10073–10081. (c) Furrer, M. A.; Schmitt, F.; Wiederkehr, M.; Juillerat-Jeanerret, L.; Therrien, B. Cellular delivery of pyrenyl-arene ruthenium complexes by a water-soluble arene ruthenium metalla-cage. *Dalton Trans.* **2012**, *41*, 7201–7211. (d) Biancalana, L.; Batchelor, L. K.; Ciancaleoni, G.; Zacchini, S.; Pampaloni, G.; Dyson, P. J.; Marchetti, F. Versatile coordination of acetazolamide to ruthenium(II)-p-cymene complexes and preliminary cytotoxicity studies. *Dalton Trans.* **2018**, *47*, 9367–9384.

(24) (a) Murray, B. S.; Babak, M. V.; Hartinger, C. G.; Dyson, P. J. The development of RAPTA compounds for the treatment of tumors. *Coord. Chem. Rev.* **2016**, *306*, 86–114 and references therein. (b) Weiss, A.; Berndsen, R. H.; Dubois, M.; Müller, C.; Schibli, R.; Griffioen, A. W.; Dyson, P. J.; Nowak-Sliwinska, P. In vivo anti-tumor activity of the organometallic ruthenium(II)-arene complex $[\text{Ru}(\eta^6\text{-p-cymene})\text{Cl}_2(\text{pta})]$ (RAPTA-C) in human ovarian and colorectal carcinomas. *Chem. Sci.* **2014**, *5*, 4742–4748. (c) Murray, B. S.; Menin, L.; Scopelliti, R.; Dyson, P. J. Conformational control of anticancer activity: the application of arene-linked dinuclear ruthenium(II)

organometallics. *Chem. Sci.* **2014**, *5*, 2536–2545. (d) Adhiresan, Z.; Davey, G. E.; Campomanes, P.; Groessl, M.; Clavel, C. M.; Yu, H.; Nazarov, A. A.; Hui Fang Yeo, C.; Ang, W. H.; Dröge, P.; Rothlisberger, U.; Dyson, P. J.; Davey, C. A. Ligand substitutions between ruthenium–cymene compounds can control protein versus DNA targeting and anticancer activity. *Nat. Commun.* **2014**, *5*, 3462.

(25) (a) Busetto, L.; Marchetti, F.; Zacchini, S.; Zanotti, V. Diiron and diruthenium aminocarbyne complexes containing pseudohalides: stereochemistry and reactivity. *Inorg. Chim. Acta* **2005**, *358*, 1204–1216. (b) Albano, V. G.; Busetto, L.; Marchetti, F.; Monari, M.; Zacchini, S.; Zanotti, V. Synthesis and Characterization of New Diiron and Diruthenium μ -Aminocarbyne Complexes Containing Terminal S-, P- and C-Ligands. *Z. Naturforsch., B: J. Chem. Sci.* **2007**, *62b*, 427–438. (c) Busetto, L.; Marchetti, F.; Salmi, M.; Zacchini, S.; Zanotti, V. Coupling of Allenes with μ -Alkylidyne Ligands in Diiron Complexes: Synthesis of Novel Bridging Thio- and Aminobutadienyldiene Complexes. *Eur. J. Inorg. Chem.* **2008**, *2008*, 2437–2447. (d) Ciancaleoni, G.; Zacchini, S.; Zanotti, V.; Marchetti, F. DFT Mechanistic Insights into the Alkyne Insertion Reaction Affording Diiron μ -Vinyliminium Complexes and New Functionalization Pathways. *Organometallics* **2018**, *37*, 3718–3731. (e) Busetto, L.; Marchetti, F.; Zacchini, S.; Zanotti, V. Reactions of Diiron μ -Aminocarbyne Complexes Containing Nitrile Ligands. *J. Braz. Chem. Soc.* **2003**, *14*, 902–907.

(26) Marchetti, F.; Zacchini, S.; Zanotti, V. Carbon monoxide–isocyanide coupling promoted by acetylide addition to a diiron complex. *Chem. Commun.* **2015**, *51*, 8101–8104.

(27) Fe complexes: (a) Mejia-Rodriguez, R.; Chong, D.; Reibenspies, J. H.; Soriaga, M. P.; Darensbourg, M. Y. The Hydrophilic Phosphatriazaadamantane Ligand in the Development of H₂ Production Electrocatalysts: Iron Hydrogenase Model Complexes. *J. Am. Chem. Soc.* **2004**, *126*, 12004–12014. (b) Wang, Z.; Liu, J.; He, C.; Jiang, S.; Akemark, B.; Sun, L. Diiron azadithiolates with hydrophilic phosphatriazaadamantane ligand as iron-only hydrogenase active site models: Synthesis, structure, and electrochemical study. *Inorg. Chim. Acta* **2007**, *360*, 2411–2419. (c) Chen, J.; Szalda, D. J.; Fujita, E.; Creutz, C. Iron(II) and Ruthenium(II) Complexes Containing P, N, and H Ligands: Structure, Spectroscopy, Electrochemistry, and Reactivity. *Inorg. Chem.* **2010**, *49*, 9380–9391.

(28) Metal compounds with an N-coordinated PTA ligand are rare, exhibiting a ³¹P signal in the range –75 to –100 ppm. (a) Smolenski, P.; Benisvy, L.; Guedes da Silva, M. F. C.; Pombeiro, A. J. L. Syntheses and Crystal Structures of the First Zinc Complex with 1,3,5-Triaza-7-phosphaadamantane (PTA), $[\text{ZnCl}_2(\text{PTA})_2]$, and of the Hybrid Organic–Inorganic Salts of N-Methyl-1,3,5-triaza-7-phosphaadamantane with Tetrahalozinc $[\text{PTA-Me}]_2[\text{ZnI}_2\text{X}_2]$ (X = I, Cl). *Eur. J. Inorg. Chem.* **2009**, *2009*, 1181–1186. (b) Jaros, S. W.; Guedes da Silva, M. F. C.; Florek, M.; Smolenski, P.; Pombeiro, A. J. L.; Kirillov, A. M. Silver(I) 1,3,5-Triaza-7-phosphaadamantane Coordination Polymers Driven by Substituted Glutarate and Malonate Building Blocks: Self-Assembly Synthesis, Structural Features, and Antimicrobial Properties. *Inorg. Chem.* **2016**, *55*, 5886–5894. (c) Mohr, F.; Falvello, L. R.; Laguna, M. A Silver(I) Coordination Polymer Containing Tridentate N- and P-Coordinating 1,3,5-Triaza-7-phosphaadamantane (PTA) Ligands. *Eur. J. Inorg. Chem.* **2006**, *2006*, 3152–3154. (d) Smoleński, P.; Kochel, A. Synthesis of the first monodentate S- and O-coordinating 1,3,5-triaza-7-phosphaadamantane-7-chalcogenides $[\text{CoCl}(\text{bpy})_2(\text{Z-PTAZ})]\text{X}$ (ZS, O; bpy = 2,2'-bipyridine; X = BF₄, PF₆) and $[\text{CoCl}(\text{bpy})_2(\text{N-PTA})]\text{BF}_4$ (PTA = 1,3,5-triaza-7-phosphaadamantane). *Polyhedron* **2010**, *29*, 1561–1566.

(29) Busetto, L.; Marchetti, F.; Zacchini, S.; Zanotti, V. Deprotonation of μ -Vinyliminium Ligands in Diiron Complexes: A Route for the Synthesis of Mono- and Polynuclear Species Containing Novel Multidentate Ligands. *Organometallics* **2005**, *24*, 2297–2306.

(30) Busetto, L.; Marchetti, F.; Zacchini, S.; Zanotti, V.; Zoli, E. Diiron-aminocarbyne complexes with amine or imine ligands: C–N coupling between imine and aminocarbyne ligands promoted by

tolyacetylide addition to aminocarbene complex. *J. Organomet. Chem.* **2005**, *690*, 348–357.

(31) (a) Singleton, M. L.; Crouthers, D. J.; Duttweiler, R. P., III; Reibenspies, J. H.; Darenbourg, M. Y. Sulfonated Diiron Complexes as Water-Soluble Models of the [Fe–Fe]-Hydrogenase Enzyme Active Site. *Inorg. Chem.* **2011**, *50*, 5015–5026. (b) Vannucci, A. K.; Wang, S.; Nichol, G. S.; Lichtenberger, D. L.; Evans, D. H.; Glass, R. S. Electronic and geometric effects of phosphatridiazadamantane ligands on the catalytic activity of an [FeFe] hydrogenase inspired complex. *Dalton Trans.* **2010**, *39*, 3050–3056.

(32) Marloye, M.; Berger, G.; Gelbcke, M.; Dufasne, F. A survey of the mechanisms of action of anticancer transition metal complexes. *Future Med. Chem.* **2016**, *8*, 2263–2286.

(33) Casey, C. P.; Marder, S. R.; Colborn, R. E.; Goodson, P. A. Conversion of Diiron Bridging Alkenyl Complexes to Monoiron Alkenyl Compounds and to Alkenes. *Organometallics* **1986**, *5*, 199–203.

(34) A second set of signals (~9%) was observed for **5a**, ascribable to the *trans* isomer: Cox, G.; Dowling, C.; Manning, A. R.; McArdle, P.; Cunningham, D. A reinvestigation of the reaction of $[\text{Fe}_2(\eta\text{-C}_3\text{H}_5)_2(\text{CO})_{4-n}(\text{CNR})_n]$ ($n = 1$ or 2) with strong alkylating agents. *J. Organomet. Chem.* **1992**, *438*, 143–158.

(35) (a) Morgan, S. E.; Kastan, M. B. p53 and ATM: cell cycle, cell death, and cancer. *Adv. Cancer Res.* **1997**, *71*, 1–25. (b) Bullock, A. N.; Fersht, A. R. Rescuing the function of mutant p53. *Nat. Rev. Cancer* **2001**, *1*, 68–76.

(36) Mazzoni, R.; Gabiccini, A.; Cesari, C.; Zanotti, V.; Gualandi, I.; Tonelli, D. Diiron Complexes Bearing Bridging Hydrocarbyl Ligands as Electrocatalysts for Proton Reduction. *Organometallics* **2015**, *34*, 3228–3235.

(37) Agonigi, G.; Ciancaleoni, G.; Funaioli, T.; Zacchini, S.; Pineider, F.; Pinzino, C.; Pampaloni, G.; Zanotti, V.; Marchetti, F. Controlled Dissociation of Iron and Cyclopentadienyl from a Diiron Complex with a Bridging C_3 Ligand Triggered by One-Electron Reduction. *Inorg. Chem.* **2018**, *57*, 15172–15186.

(38) Rocco, D.; Batchelor, L. K.; Ferretti, E.; Zacchini, S.; Pampaloni, G.; Dyson, P. J.; Marchetti, F. Piano Stool Aminoalkylidene-Ferracyclopentenone Complexes from Bimetallic Precursors: Synthesis and Cytotoxicity Data. *ChemPlusChem* **2020**, *85*, 110–122.

(39) Schroeder, N. C.; Angelici, R. J. Synthesis and Reactivity of the Bridging Thiocarbonyl Radical, $\text{Cp}_2\text{Fe}_2(\text{CO})_2(\mu\text{-CO})(\mu\text{-CSMe})$. *J. Am. Chem. Soc.* **1986**, *108*, 3688–3693.

(40) Zanotti, V.; Bordoni, S.; Busetto, L.; Carlucci, L.; Palazzi, A.; Serra, R.; Albano, V. G.; Monari, M.; Prestopino, F.; Laschi, F.; Zanello, P. Diiron Aminoalkylidene Complexes. *Organometallics* **1995**, *14*, 5232–5241.

(41) The analogue of **9b**, bearing two methyl N substituents, was reported to display a reversible redox process on the anodic side at +0.21 V (vs Fc/Fc⁺, MeCN solution).

(42) (a) Leonidova, A.; Anstaett, P.; Pierroz, V.; Mari, C.; Spingler, B.; Ferrari, S.; Gasser, G. Induction of Cytotoxicity through Photorelease of Aminoferrrocene. *Inorg. Chem.* **2015**, *54*, 9740–9748. (b) Marzenell, P.; Hagen, H.; Sellner, L.; Zenz, T.; Grinyte, R.; Pavlov, V.; Daum, S.; Mokhir, A. Aminoferrrocene-Based Prodrugs and Their Effects on Human Normal and Cancer Cells as Well as Bacterial Cells. *J. Med. Chem.* **2013**, *56*, 6935–6944.

(43) Schafer, F. Q.; Buettner, G. R. Redox environment of the cell as viewed through the redox state of the glutathione disulfide/glutathione couple. *Free Radical Biol. Med.* **2001**, *30*, 1191–1212.

(44) (a) Fu, Y.; Romero, M. J.; Habtemariam, A.; Snowden, M. E.; Song, L.; Clarkson, G. J.; Qamar, B.; Pizarro, A. M.; Unwin, P. R.; Sadler, P. J. The contrasting chemical reactivity of potent isoelectronic iminopyridine and azopyridine osmium(II) arene anticancer complexes. *Chem. Sci.* **2012**, *3*, 2485–2493. (b) Du, Q.; Guo, L.; Tian, M.; Ge, X.; Yang, Y.; Jian, X.; Xu, Z.; Tian, Z.; Liu, Z. Potent Half-Sandwich Iridium(III) and Ruthenium(II) Anticancer Complexes Containing a P=O-Chelated Ligand. *Organometallics* **2018**, *37*, 2880–2889.

(45) Giordano, C.; Montopoli, M.; Perli, E.; Orlandi, M.; Fantin, M.; Ross-Cisneros, F. N.; Caparrotta, L.; Martinuzzi, A.; Ragazzi, E.; Ghelli, A.; Sadun, A. A.; d'Amati, G.; Carelli, V. Oestrogens ameliorate mitochondrial dysfunction in Leber's hereditary optic neuropathy. *Brain* **2011**, *134*, 220–234.

(46) Lackowicz, J. R. *Principles of fluorescence Spectroscopy*, 3rd ed.; Springer: 2006.

(47) Nissani, E.; Perlmutter-Hayman, B. Drug-binding to biological macromolecules. A kinetic study of the system chlorodiazepoxide (librium) and bovine serum albumin. *Int. J. Chem. Kinet.* **1986**, *18*, 1123–1132.

(48) Selected references: (a) Foresti, R.; Bani-Hani, M. G.; Motterlini, R. Use of carbon monoxide as a therapeutic agent: promises and challenges. *Intensive Care Med.* **2008**, *34*, 649–658. (b) Kawahara, B.; Moller, T.; Hu-Moore, K.; Carrington, S.; Faull, K. F.; Sen, S.; Mascharak, P. K. Attenuation of Antioxidant Capacity in Human Breast Cancer Cells by Carbon Monoxide through Inhibition of Cystathionine β -Synthase Activity: Implications in Chemotherapeutic Drug Sensitivity. *J. Med. Chem.* **2017**, *60*, 8000–8010. (c) Motterlini, R.; Otterbein, L. E. The therapeutic potential of carbon monoxide. *Nat. Rev. Drug Discovery* **2010**, *9*, 728. (d) Mann, B. E. CO-Releasing Molecules: A Personal View. *Organometallics* **2012**, *31*, 5728–5735. (e) Ji, X.; Wang, B. Strategies toward Organic Carbon Monoxide Prodrugs. *Acc. Chem. Res.* **2018**, *51*, 1377–1385.

(49) Fulmer, G. R.; Miller, A. J. M.; Sherden, N. H.; Gottlieb, H. E.; Nudelman, A.; Stoltz, B. M.; Bercaw, J. E.; Goldberg, K. I. NMR Chemical Shifts of Trace Impurities: Common Laboratory Solvents, Organics, and Gases in Deuterated Solvents Relevant to the Organometallic Chemist. *Organometallics* **2010**, *29*, 2176–2179.

(50) Willker, W.; Leibfritz, D.; Kerssebaum, R.; Bermel, W. Gradient selection in inverse heteronuclear correlation spectroscopy. *Magn. Reson. Chem.* **1993**, *31*, 287–292.

(51) Sheldrick, G. M. SADABS-2008/1-Bruker AXS Area Detector Scaling and Absorption Correction; Bruker AXS: Madison, WI, USA, 2008.

(52) Sheldrick, G. M. Crystal structure refinement with SHELXL. *Acta Crystallogr., Sect. C: Struct. Chem.* **2015**, *71*, 3.

(53) Rundlöf, T.; Mathiasson, M.; Bekiroglu, S.; Hakkarainen, B.; Bowden, T.; Arvidsson, T. Survey and qualification of internal standards for quantification by ^1H NMR spectroscopy. *J. Pharm. Biomed. Anal.* **2010**, *52*, 645–651.

(54) Rice, N. M.; Irving, H. M. N. H.; Leonard, M. A. Nomenclature for liquid-liquid distribution (solvent extraction) (IUPAC Recommendations 1993). *Pure Appl. Chem.* **1993**, *65*, 2373–2396.

(55) (a) *OECD Guidelines for Testing of Chemicals*; OECD: Paris, 1995; Vol. 107. (b) Dearden, J. C.; Bresnen, G. M. The Measurement of Partition Coefficients. *Quant. Struct.-Act. Relat.* **1988**, *7*, 133–144. (c) Biancalana, L.; Batchelor, L. K.; Funaioli, T.; Zacchini, S.; Bortoluzzi, M.; Pampaloni, G.; Dyson, P. J.; Marchetti, F. α -Diimines as Versatile, Derivatizable Ligands in Ruthenium(II) p-Cymene Anticancer Complexes. *Inorg. Chem.* **2018**, *57*, 6669–6685.

(56) Rimoldi, I.; Facchetti, G.; Lucchini, G.; Castiglioni, E.; Marchianò, S.; Ferri, N. *In vitro* anticancer activity evaluation of new cationic platinum(II) complexes based on imidazole moiety. *Bioorg. Med. Chem.* **2017**, *25*, 1907–1913.

(57) Cerchiaro, G.; Manieri, T. M.; Bertuchi, F. R. Analytical methods for copper, zinc and iron quantification in mammalian cells. *Metallomics* **2013**, *5*, 1336–1345.

(58) Biver, T.; Secco, F.; Tinè, M. R.; Venturini, M.; Bencini, A.; Bianchi, A.; Giorgi, C. Intercalation of Zn(II) and Cu(II) complexes of the cyclic polyamine Neotrien into DNA: equilibria and kinetics. *J. Inorg. Biochem.* **2004**, *98*, 1531–1538.

(59) Marzo, T.; Cirri, D.; Ciofi, L.; Gabbiani, C.; Feis, A.; Di Pasquale, N.; Stefanini, M.; Biver, T.; Messori, L. Synthesis, characterization and DNA interactions of $[\text{Pt}_3(\text{TPyMT})\text{Cl}_3]$, the trinuclear platinum(II) complex of the TPymT ligand. *J. Inorg. Biochem.* **2018**, *183*, 101–106.